

Aperiodic-sampled neural network controllers with closed-loop stability verifications (extended version)

Renjie Ma^{a,b}, Zhijian Hu^c, Rongni Yang^d, Ligang Wu^e

^aState Key Laboratory of Robotics and Systems, Harbin Institute of Technology, Harbin 150001, China

^bChongqing Research Institute, Harbin Institute of Technology, Chongqing 401120, China

^cLAAS-CNRS, University of Toulouse, CNRS, Toulouse 31077, France

^dSchool of Control Science and Engineering, Shandong University, Jinan 250061, China

^eSchool of Astronautics, Harbin Institute of Technology, Harbin 150001, China

Abstract

In this paper, we synthesize two aperiodic-sampled deep neural network (DNN) control schemes, based on the closed-loop tracking stability guarantees. By means of the integral quadratic constraint coping with the input-output behaviour of system uncertainties/nonlinearities and the convex relaxations of nonlinear DNN activations leveraging their local sector-bounded attributes, we establish conditions to design the event- and self-triggered logics and to compute the ellipsoidal inner approximations of region of attraction, respectively. Finally, we perform a numerical example of an inverted pendulum to illustrate the effectiveness of the proposed aperiodic-sampled DNN control schemes.

Key words: Aperiodic-sampled scheme; stability analysis; deep neural network; robust control; region of attraction estimation

1 Introduction

The rapid developments of imitation learning motivate new perspectives of control designs for cyber-physical systems. Apart from minimizing a loss function based on exploration-exploitation tradeoffs (Jin & Lavaei, 2018), learning a control strategy to obtain the prescribed system performances and to imitate the expert demonstrations has obtained eye-catching achievements in recent years (Yin, Seiler, Jin, & Arcak, 2022b). Within this context, deep neural networks (DNNs) can be utilized to displace computation-expensive control policies, such as model predictive control, and to

present better adaptivity to uncertainties and less conservatism (Karg & Lucia, 2020). However, providing a theoretical guarantee of learned behaviour is challenging, due to the nonlinear and large-scale attributes of DNN, which limits practical applications of neural-feedback loops.

1.1 Related Literature

The numerous hidden layers and neurons, as well as nonlinear DNN activation functions bring challenges for system analysis (La Bella, Farina, D'Amico, & Zaccarian, 2025; Nino, Patil, Insinger, Eisman, & Dixon, 2025). Thus, the convex relaxations of DNNs are crucial for deriving theoretical guarantees of neural-feedback loops. For example, the Lipschitz continuity of DNNs (D'Amico, La Bella, & Farina, 2024; Fazlyab, Robey, Hassani, Morari, & Pappas, 2019; Pauli, Koch, Berberich, Kohler, & Allgöwer, 2021b) is a common assumption, and the Lipschitz constant provides an upper bound on the degrees of DNN output changes, which can be incorporated into the Lyapunov-based system analysis (Talukder & Kumar, 2023). Particularly, the LipSDP algorithm (Fazlyab, Robey, Hassani, Morari, & Pappas, 2019) computes tight estimations of upper bounds on the Lipschitz constant of DNNs, based on the slope-restricted attribute of activation functions. Then, the work (Pauli, Koch,

* This paper was supported in part by the National Key Research and Development Program of China under Grant 2023YFE02099 00, the National Natural Science Foundation of China under Grants 62033005, 62320106001, and 62273208, the Natural Science Foundation of Heilongjiang Province under Grant LH2024F026, and the Natural Science Foundation of Chongqing Municipality under Grant CSTB2023NSCQ-MSX0625.

**This paper was not presented at any IFAC meeting. Corresponding author: Ligang Wu.

Email addresses: renjiema@hit.edu.cn (Renjie Ma), zhijian.hu@ntu.edu.sg (Zhijian Hu), rnyang@sdu.edu.cn (Rongni Yang), ligangwu@hit.edu.cn (Ligang Wu).

Berberich, Kohler, & Allgöwer, 2021b) proposes an optimization framework to train a DNN and to promote its robustness with a small Lipschitz constant. Note that the specific nonlinear attributes of activation functions are crucial for relaxing DNNs, such as linear programming (Wong & Kolter, 2018) and semidefinite programming (Raghuathan, Steinhardt, & Liang, 2018) methods for ReLU DNNs. In general, slope restrictions and sector bounds are commonly utilized to abstract nonlinear DNN activation functions by virtue of quadratic constraints (Fazlyab, Morari, & Pappas, 2022; Ma & Hu, 2024), which lead to sufficient conditions of stability guarantee based on linear matrix inequalities. Accordingly, robust ellipsoidal inner approximations of region of attraction (RoA) can be obtained for uncertain neural-feedback loops with perturbations formulated by integral quadratic constraints (IQCs) in (Yin, Seiler, & Arcak, 2022a) and (Pauli, Köhler, Berberich, Koch, & Allgöwer, 2021a). Besides, quadratic constraints of DNNs can also be used for analyzing the forward reachability of neural-feedback loops by semidefinite programming in both centralized (Hu, Fazlyab, Morari, & Pappas, 2020) and distributed (Gates, Newton, & Gatsis, 2023) scenarios. Moreover, interval arithmetic frameworks of DNNs can be incorporated into a simulation-guided reachability analysis (Xiang, Tran, Yang, & Johnson, 2021) or be involved in a mixed-integer linear programming to obtain the closed-loop stability guarantees (Fabiani & Goulart, 2023).

Periodic time-triggered sampling schemes are not resource-efficient in the sense of networked control (Heemels, Johansson, & Tabuada, 2012). Enabling communication transmissions only when necessary can refine unnecessary waste of communication resources, which motivates the developments of event- and self-triggered control. Based on continuous monitoring of system states, an event trigger can check whether the state value has changed and satisfied the specific logic, and can authorize the communication transmissions to update control inputs (Hu, Su, Veerasamy, Huang, & Ma, 2025; Seuret, 2012). The core of event-triggered control (ETC) lies in specifying a triggering logic incorporated into a control strategy such that the desired closed-loop performances can be guaranteed. Normally, a triggering logic relies on the Lyapunov function (Ghodrat & Marquez, 2023) or the error signal (Coutinho & Palhares, 2022; Girard, 2015; Liu, Wang, He, & Zhou, 2015; Seifullae, Knorn, & Ahlén, 2022; Tripathy, Kar, & Paul, 2017; Ye, Song, Zhang, & Wen, 2023; Zhao, Zuo, & Wang, 2022). Compared with static ETC, both the state trajectory and the auxiliary variable need to be converged synchronously for dynamic ETC, which potentially enlarges the minimum inter-execution time (Girard, 2015). For a self-triggered control (STC) scheme, the crux is to compute the upcoming transmission instant, by virtue of the transmitted signals, in advance (Akashi, Ishii, & Cetinkaya, 2018). Therefore, a continuous event detector for monitoring system state is unnecessary, and the communication transmission is shut until the upcoming triggering instant. Extensive applications of STC are widely emerged in quantized control (Wakaiki, 2023), resilient control against communication delays and packet

dropouts (Peng & Han, 2016), nonlinear control (Li, Wang, & Song, 2023), switched control (Cao, Niu, & Zou, 2023; Wan, Luan, Karimi, & Liu, 2021), and data-driven control (Wang, Berberich, Sun, Wang, Allgöwer, & Chen, 2023; Wildhagen, Berberich, Hertneck, & Allgöwer, 2023), where both closed-loop stability guarantees and STC syntheses are performed together. Fewer results have explored DNN-based ETC and STC schemes, compared to time-triggered DNN controllers (Gates, Newton, & Gatsis, 2023; Hu, Fazlyab, Morari, & Pappas, 2020; Pauli, Köhler, Berberich, Koch, & Allgöwer, 2021a; Yin, Seiler, & Arcak, 2022a), which acts as the first motivation of this paper.

The uncertainty impacts, such as unmodeled dynamics, time delays, and adversarial attacks/faults (Ma, Shi, & Wu, 2021), inevitably degrade closed-loop performances of neural-feedback loops, in view of the intrinsic vulnerability of DNNs (Fazlyab, Morari, & Pappas, 2022). Enhancing resilience of neural-feedback loops in the sense of robust control is critically important. Integral quadratic constraints (IQCs) can describe the local input-output behaviour of a general uncertainty, which interconnects in feedback with a nominal system (Seiler, 2015). IQCs cover a multitude of uncertainties and nonlinearities in the time domain (Lessard, Recht, & Packard, 2016) and perform less conservatism for deriving closed-loop performance guarantees (Schwenkel, Köhler, Müller, & Allgöwer, 2023). Due to the nonlinearity attribute of neural-feedback loops, the stabilization control is normally not in the global sense. The size of region of attraction (RoA), acting as a stability metric, can be utilized to assess the effectiveness of specified control policy. In practice, computing an exact RoA to obtain its complicated analytical expression is difficult, therefore, many algorithms have been developed to obtain inner approximations of RoA in view of sublevel sets of Lyapunov functions (Iannelli, Seiler, & Marcos, 2019; Valmorbidia & Anderson, 2017), in which nonrestrictive IQCs can be well involved. However, fewer results have revealed inner approximations of RoA for neural-feedback loops with aperiodic-sampled communication between sensor and controller, which acts as the second motivation of this paper.

1.2 Technical Contributions

In this paper, we aim at filling the gap between aperiodic-sampled communication transmissions and neural-feedback loops. Note that the technical results herein are different from the existing literature. First, establishing the relationships between the triggering parameters and the size of robust inner approximation of RoA, were not revealed in (Yin, Seiler, & Arcak, 2022a). Besides, the triggering mechanisms herein are theoretically different from the counterpart in (de Souza, Girard, & Tarbouriech, 2023), where the event triggers are located within the interior of a DNN. Although the work (Wang, Berberich, Sun, Wang, Allgöwer, & Chen, 2023) provides promising tools for aperiodic-sampled controller designs for linear systems, it cannot be used directly toward neural-feedback loops, due to intrinsically nonlinear

DNN activations. In addition, the stability-guaranteed STC synthesis, connecting self-triggered logics with closed-loop performances, was not developed therein. The main contributions of this paper are summarized by the following points.

- The resource-efficient event- and self-triggered communication schemes are deployed with the channel between the sampler and the DNN controller, such that the triggering time instants can be autonomously determined by monitoring the state trajectories of neural-feedback loops, rather than the preactivation and activation of each DNN layer, which reduces communication and computation burdens.
- Based on the quadratic constraint of DNN induced by the local attributes of repeated activation function and the auxiliary looped functions, the sufficient conditions on ensuring the setpoint tracking stability of aperiodic-sampled neural-feedback loops with less conservatism can be derived.
- The size of ellipsoidal inner approximation of RoA in the sense of robust control is extracted as a stability metric, which closely associates with the triggering parameters. By solving the proposed semidefinite programming problems, the triggering parameters can be determined on the premise of enlarging the RoA inner approximation.

1.3 Outline of This Paper

The problem formulation is stated in Section 2. Then the event-triggered and self-triggered DNN controller designs together with the closed-loop stability analyses are put forward in Sections 3 and 4, respectively. Section 5 exhibits an example of an inverted pendulum to validate the effectiveness of proposed theoretical results. We conclude this paper in Section 6.

1.4 Applicatory Notations

\mathbb{S}^n denotes the set of n -by- n symmetric matrices. $\mathbb{RL}_\infty^{m \times p}$ denotes the set of m -by- p real-rational and proper transfer matrices, with no poles on the unit circle. Its subset $\mathbb{RH}_\infty^{m \times p}$ contains functions which are analytic outside the closed unit disk. We define the set of sequence in \mathbb{R}^n by $\ell_{2e}^n = \{(v(k)), k \in \mathbb{N} | v(k) \in \mathbb{R}^n\}$. $\mathbb{N}_{[r_1, r_2]} \subseteq \mathbb{N}$ denotes the nonnegative integer set $\{r_1, r_1+1, \dots, r_2\}$ with $r_2 > r_1 \geq 0$. We denote the positive (semi-) definite and symmetric matrix by $Q \succ \mathbf{0} (\succeq \mathbf{0})$, and $\|v_k\|_Q^2$ equals to $v_k^\top Q v_k$. $\text{Det}(R)$ captures the determinant of symmetric matrix R . The column-arranged matrix/vector $[L_1^\top, \dots, L_{r_1}^\top]^\top$ is depicted by $\text{Col}(L_1, \dots, L_{r_1})$. $\text{Diag}(H_1, \dots, H_{r_2})$ denotes the symmetric matrix whose diagonal elements are $H_i, i \in \mathbb{N}_{[1, r_2]}$.

2 Problem Formulation

We consider a discrete-time control system $F(\Gamma, \Theta)$ with an interconnection of a nominal plant Γ and an uncertainty part Θ (Hu, Lacerda, & Seiler, 2017). For sampling time instant $k \in \mathbb{N}$, the nominal plant Γ can be described by

$$\begin{aligned} x(k+1) &= A_\Gamma x(k) + B_\Gamma u(k) + F_\Gamma \omega(k), \\ \nu(k) &= C_\Gamma x(k) + D_\Gamma u(k) + G_\Gamma \omega(k), \end{aligned} \quad (1)$$

where $x \in \mathbb{R}^n$ denotes the system state, $u \in \mathbb{R}^m$ denotes the control input, $\nu \in \mathbb{R}^v$ and $\omega \in \mathbb{R}^w$ represent the input and output of the uncertainty part Θ , respectively. We assume that the system matrices of (1) are known with suitable dimensions.

The nominal plant Γ is interconnected in feedback with a bounded and casual operator $\Theta: \ell_{2e}^v \mapsto \ell_{2e}^w$ formulated by

$$\omega(k) = \Theta(\nu(k)). \quad (2)$$

We assume that the interconnection of Γ and Θ is well-posed, namely, there exist the unique response $x \in \ell_{2e}^n$, $\omega \in \ell_{2e}^w$, $\nu \in \ell_{2e}^v$ for each $u \in \ell_{2e}^m$, which guarantees that the control system $F(\Gamma, \Theta)$ has the unique solution, and there is no algebraic loop for the interconnection of Γ and Θ (Schwenkel, Köhler, Müller, & Allgöwer, 2023). Besides, all state measurements x are available for feedback control.

IQCs exhibit powerful effectiveness for analyzing the interconnection in feedback between Γ and Θ , which is extended to time-domain cases by dissipation inequalities (Seiler, 2015). The keypoint of characterizing the input-output relationship of uncertainty operator Θ with IQC lies in constructing a virtual filter Φ_Θ , whose state ξ relates to the input ν and the output ω of Θ , and output r leads to a quadratic constraint. The filter Φ_Θ can be described with the form

$$\begin{aligned} \xi(k+1) &= A_\Phi \xi(k) + B_\Phi \nu(k) + F_\Phi \omega(k), \\ r(k) &= C_\Phi \xi(k) + D_\Phi \nu(k) + G_\Phi \omega(k), \end{aligned} \quad (3)$$

where $\xi \in \mathbb{R}^\psi$ with $\xi(0) = 0$ and $r \in \mathbb{R}^\kappa$. It is intuitive that the filter parameters in (3) are with proper dimensions. A_Φ implies a Schur matrix, whose spectrum is contained in the open unit disk in the complex plane, ensuring that (3) has a unique solution (ξ_*, r_*) for any choice of (ν_*, ω_*) , see (Lessard, Recht, & Packard, 2016, Subsection 3.1) for more technical details. The definition of time-domain ρ -hard IQC is recapped in what follows.

Definition 1 (Lessard, Recht, & Packard, 2016) For a scalar $\rho \in \mathbb{R}_{(0,1]}$, a matrix $M_\Theta \in \mathbb{S}^\kappa$, as well as a function $\Phi_\Theta \in \mathbb{RH}_\infty^{\kappa \times (v+w)}$, the bounded and casual operator Θ defined in (2) satisfies the ρ -hard IQC described by (Φ_Θ, M_Θ) , if for all $\nu \in \ell_{2e}^v$ with $\omega = \Theta(\nu)$, and for all $\mathcal{I} \in \mathbb{N}_+$, we have

$$\sum_{k=0}^{\mathcal{I}} \rho^{-2k} r^\top(k) M_\Theta r(k) \geq 0. \quad (4)$$

We denote the augmented state by $\eta = \text{Col}(x, \xi)$ with $\eta \in \mathbb{R}^z$ and $z = n + \psi$. Then, in terms of (1) and (3), we can obtain

the augmented dynamics with the form

$$\begin{aligned} \eta(k+1) &= A\eta(k) + B\bar{u}(k), \\ r(k) &= C\eta(k) + D\bar{u}(k), \end{aligned} \quad (5)$$

where $\bar{u} = \text{Col}(u, \omega)$ and

$$\begin{aligned} A &\triangleq \begin{bmatrix} A_\Gamma & \mathbf{0} \\ B_\Phi C_\Gamma & A_\Phi \end{bmatrix}, B \triangleq \begin{bmatrix} B_\Gamma & F_\Gamma \\ B_\Phi D_\Gamma & B_\Phi G_\Gamma + F_\Phi \end{bmatrix}, \\ C &\triangleq \begin{bmatrix} D_\Phi C_\Gamma & C_\Phi \end{bmatrix}, D \triangleq \begin{bmatrix} D_\Phi D_\Gamma & D_\Phi G_\Gamma + G_\Phi \end{bmatrix}. \end{aligned}$$

The stable equilibrium of augmented system (5) is denoted by $\eta^* = \text{Col}(x^*, \xi^*)$. We let $\chi(k, x_0, \Theta)$ denote the state response of neural-feedback loops $F(\Gamma, \Theta)$ starting from the initial state $x_0 = x(0)$. It is unlikely to have a global stabilizing DNN controller, and mostly, local stability guarantees corresponding to the specific data region are sufficient (Pauli, Köhler, Berberich, Koch, & Allgöwer, 2021a). Hence, we assume that $\chi(k, x_0, \Theta)$ can converge to the stable equilibrium x^* locally, which yields the definition of robust RoA.

Definition 2 Let \mathcal{S} denote the set of uncertainty impact Θ , that is, $\Theta \in \mathcal{S}$, then the robust RoA of DNN-controlled system (5) is defined by

$$\mathcal{R}_F^x = \{x_0 \in \mathbb{R}^n \mid \lim_{k \rightarrow \infty} \chi(k, x_0, \Theta) = x^*, \forall \Theta \in \mathcal{S}\}. \quad (6)$$

The control input u can be obtained by an l -layer feed-forward DNN $\pi_{\text{DNN}}(x): \mathbb{R}^n \mapsto \mathbb{R}^m$ with the form

$$\begin{aligned} m_0(k) &= x(k), \\ m_i(k) &= \varphi_i(W_i m_{i-1}(k) + b_i), i \in \mathbb{N}_{[1, l]}, \\ u(k) &= W_{l+1} m_l(k) + b_{l+1}, \end{aligned} \quad (7)$$

where $m_i \in \mathbb{R}^{a_i}$ denotes the activation of i -th layer with $a_0 = n$, and the perception of i -th layer is attained by the weight matrix W_i and the bias b_i . The activation function φ_i is element-wise, that is,

$$\varphi_i(\mathbf{v}) = \text{Col}(s(\mathbf{v}_1), s(\mathbf{v}_2), \dots, s(\mathbf{v}_{a_i})), \quad (8)$$

where s implies a scalar nonlinear function satisfying $s(0) = 0$, which can be selected as ReLU, sigmoid, and softmax. Normally, ψ is assumed to be identical for all layers without loss of generality.

We consider that the system state is sampled and transmitted to the controller at specific time instant $k_q \in \mathbb{N}$, where $k_0 = 0$ and $k_{q+1} - k_q \geq 1$ hold for $q \in \mathbb{N}$. The available sampled state $x(k_q)$ is transmitted into π_{DNN} and leads to the control input $u(k) = \pi_{\text{DNN}}(x(k_q))$ for $k \in \mathbb{N}_{[k_q, k_{q+1}-1]}$, in

view of the zero-order hold (ZOH). To improve the communication efficiency, we will design ETC and STC schemes for neural-feedback loops (5), on the premise of the closed-loop stability guarantees.

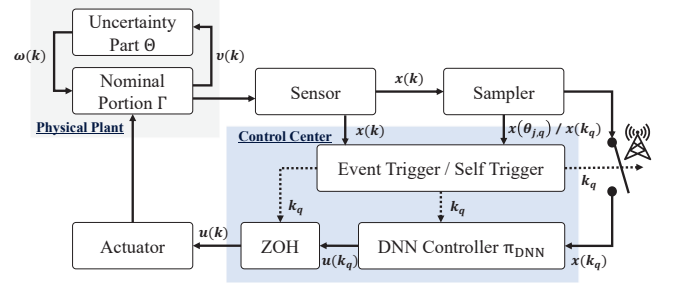


Fig. 1. The design schematic of aperiodic-sampled neural-feedback loops.

We illustrate the schematic of aperiodic-sampled neural-feedback loops $F(\Gamma, \Theta)$ in Fig. 1, based on which, the input $\bar{u}(k)$ of neural-feedback loops (5) is formulated by

$$\bar{u}(k) = \text{Col}(\pi_{\text{DNN}}(x(k_q)), \omega(k)), k \in \mathbb{N}_{[k_q, k_{q+1}-1]}. \quad (9)$$

Hence, the aperiodic-sampled DNN controller (9) depends on both the DNN architecture (7) and the adaptive triggering time instant k_q . According to Fig. 1, the transmission switch is located in the channel between the sampler and the controller, leading to aperiodic-sampled DNN control schemes (9), and the triggering time instants are autonomously determined by the state trajectory of neural-feedback loops via an event/self trigger. In contrast, the work (de Souza, Girard, & Tarbouriech, 2023) deploys an event-triggered transmission scheme in the channel between two coterminous DNN layers, and the triggering logic is based on the quadratic constraint with regard to the preactivation and activation of each layer. The number of event triggers equals to that of DNN layers therein, which implies a more complex structure than our results. The problems of interests of this paper are summarized by the following aspects.

- We deploy two effective aperiodic-sampled transmission schemes to autonomously determine the triggering instants in the channel between the sampler and the DNN controller, and to mitigate communication and computation burdens.
- We derive the closed-loop stability guarantees of aperiodic-sampled neural-feedback loops, in the light of the convex relaxations of DNN and the auxiliary looped functions combined with Lyapunov functions.
- We assess the stability metric by virtue of maximizing the inner approximation of robust RoA influenced by aperiodic-sampled schemes, and determine the triggering parameters based on the feasibility of proposed convex programming.

3 Event-Triggered Neural Control Policy

3.1 Event-Triggered Scheme

The blue rectangle within Fig. 1 depicts an event-triggered DNN controller module, where the communication time instants are captured by $\{k_q\}_{q \in \mathbb{N}}$. For ETC, the state trajectory is sampled periodically at discrete time instants $\{k_q + j\vartheta\}$ with $j \in \mathbb{N}$ and the constant sampling interval $\vartheta \in \mathbb{R}_{[\vartheta_l, \vartheta_u]}$, in which ϑ_l and $\vartheta_u \in \mathbb{N}_{\geq 1}$ are the lower and upper bounds, respectively. The following triggering rule is assessed in terms of the sampled state $x(k_q + j\vartheta)$

$$\alpha(\theta_{j,q}) + g\beta(\theta_{j,q}) < 0, \quad (10)$$

where $g \in \mathbb{R}_{\geq 0}$ is a parameter to be determined, $\theta_{j,q} \triangleq k_q + j\vartheta$ holds for $j \in \mathbb{N}_{[0, h(q)]}$ with $h(q) \triangleq (k_{q+1} - k_q)/\vartheta - 1$, $\beta(\theta_{j,q})$ defines a quadratic function around x^* with the form

$$\beta(\theta_{j,q}) = \epsilon_1 \|x(\theta_{j,q}) - x^*\|_{\Xi_1}^2 + \epsilon_2 \|x(k_q) - x^*\|_{\Xi_1}^2 - \|e(\theta_{j,q})\|_{\Xi_2}^2, \quad (11)$$

where $\epsilon_1, \epsilon_2 \in \mathbb{R}_{[0,1]}$ are triggering discount parameters, and $\Xi_1, \Xi_2 \in \mathbb{S}_{>0}^n$ are weight matrices. The error between the state trajectory $x(\theta_{j,q})$ at the current time instant and the counterpart $x(k_q)$ at the latest transmission instant is defined by $e(\theta_{j,q})$, that is, $e(\theta_{j,q}) \triangleq x(\theta_{j,q}) - x(k_q)$. Moreover, $\alpha(t)$ formulates a dynamic parameter with $\alpha(k) = \alpha(\theta_{j,q})$ and

$$\alpha(\theta_{j+1,q}) = (1 - \mu)\alpha(\theta_{j,q}) + \beta(\theta_{j,q}), \quad (12)$$

where $\alpha(0) \in \mathbb{R}_{\geq 0}$ and $\mu \in \mathbb{R}_{[0,1]}$ are prescribed coefficients.

The sampled state $x(\theta_{j,q})$ can be transmitted into the DNN controller π_{DNN} once the event-triggered logic (10) is violated. We can obtain the newly computed DNN control input held by a ZOH for the subsequent triggering interval $[k_{q+1}, k_{q+2} - 1]$, where the latest transmitted state is used to update the event-triggered DNN control input, and accordingly, to determine the next sampled state. Thus, the dynamic event-triggered logic is formulated by

$$k_{q+1} = k_q + \vartheta \min_j \{j \in \mathbb{N}_+ | \alpha(\theta_{j,q}) + g\beta(\theta_{j,q}) < 0\}. \quad (13)$$

Remark 1 *Once the event-triggered condition (10) is violated, we have $\alpha(\theta_{j,q}) + g\beta(\theta_{j,q}) \geq 0$. For $g=0$, $\alpha(\theta_{j,q}) \geq 0$ holds. While for $g \in \mathbb{R}_{>0}$, $\beta(\theta_{j,q}) \geq -\alpha(\theta_{j,q})/g$ holds, then based on which, (12) leads to $\alpha(\theta_{j+1,q}) \geq (1 - \mu - g^{-1})\alpha(\theta_{j,q})$. Thus, $\alpha(\theta_{j,q}) \geq 0$ holds for any $j \in \mathbb{N}_{[0, h(q)]}$ on the premise of both the initial condition $\alpha(0) \geq 0$ and the prerequisite constraint $1 - \mu - g^{-1} \geq 0$ (Wang, Berberich, Sun, Wang, Allgöwer, & Chen, 2023). Hence, the nonnegativity of $\alpha(\theta_{j,q})$ is satisfied when deploying the event-triggered scheme (13).*

Remark 2 *In essence, the deployed event-triggered scheme (13) is more general. For example, it can boil down to the dynamic triggering logic established in (Girard, 2015), if $\vartheta = g = 1$, $\epsilon_1 = 1$, and $\epsilon_2 = 0$ hold for (11). In addition, it can further cover the static triggering logics (Ghodrat & Marquez, 2023; Seifullaev, Knorn, & Ahlén, 2022; Tripathy, Kar, & Paul, 2017; Zhao, Zuo, & Wang, 2022) without the consideration of the non-negative $\alpha(\theta_{j,q})$. Besides, if we set $\epsilon_1 = \epsilon_2 = 0$, then the condition (10) leads to the triggering scheme developed by (Liu, Wang, He, & Zhou, 2015). Moreover, compared to (Wang, Berberich, Sun, Wang, Allgöwer, & Chen, 2023), different weight parameters Ξ_1 and Ξ_2 embedded in $\beta(\theta_{j,q})$ can incorporate more general triggering conditions in (Girard, 2015; Tripathy, Kar, & Paul, 2017) better. Hence, the conducted triggering scheme (13) potentially unifies and generalizes most of existing event-triggered mechanisms.*

3.2 Convex Relaxation of Deep Neural Network

We define the DNN preactivations by $p_i(k) = W_i m_{i-1}(k) + b_i$, such that $m_i(k) = \varphi_i(p_i(k))$ holds for $i \in \mathbb{N}_{[1, l]}$. Hence, by aggregating the inputs and outputs of the activation layers with $\mathbf{g} = \text{Col}(\mathbf{g}_1, \dots, \mathbf{g}_l) \in \mathbb{R}^a$, $a = \sum_{i=1}^l a_i$, in which \mathbf{g} can be p and m , respectively, the condition $m = \varphi(p)$ holds element-wisely for repeated nonlinearities (8). The nonlinearities can be isolated based on (7) combined with the superposition of linear operator (Fazlyab, Morari, & Pappas, 2022), which yields

$$\begin{bmatrix} u(k) \\ p(k) \end{bmatrix} = \begin{bmatrix} \Pi_{ux} & \Pi_{um} & \Pi_{u1} \\ \Pi_{px} & \Pi_{pm} & \Pi_{p1} \end{bmatrix} \begin{bmatrix} x(k_q) \\ m(k) \\ 1 \end{bmatrix}, m(k) = \varphi(p(k)), \quad (14)$$

for the time instant $k \in \mathbb{N}_{[k_q, k_{q+1} - 1]}$, and

$$\begin{aligned} \Pi_{ux} &\triangleq \mathbf{0}_{m \times n}, \Pi_{um} \triangleq \begin{bmatrix} \mathbf{0}_{m \times \mathcal{Z}(a_1, a_{l-1})} & W_{l+1} \end{bmatrix}, \Pi_{u1} \triangleq b_{l+1}, \\ \Pi_{px} &\triangleq \text{Col}(W_1, \mathbf{0}_{\mathcal{Z}(a_2, a_l) \times n}), \Pi_{p1} \triangleq \text{Col}(b_1, b_2, \dots, b_l), \\ \Pi_{pm} &\triangleq \text{Col}(\mathbf{0}_{a_1 \times \mathcal{Z}(a_1, a_l)}, \tilde{\Pi}_{pm}), \tilde{\Pi}_{pm} \triangleq \begin{bmatrix} \tilde{\Pi}_{pm}^{(1)} & \mathbf{0}_{\mathcal{Z}(a_2, a_l) \times a_l} \end{bmatrix}, \\ \tilde{\Pi}_{pm}^{(1)} &\triangleq \text{Diag}(W_2, W_3, \dots, W_l), \end{aligned} \quad (15)$$

holding with $\mathcal{Z}(a_i, a_j) = \sum_{\kappa=i}^j a_\kappa$. The repeated nonlinearities (8) normally satisfy the sector-bounded or/and slope-restricted properties, which can be potentially utilized to relax π_{DNN} by performing quadratic constraints based on (14).

Note that the global sector bounds of an activation function are too conservative to assess the closed-loop stability in a more exact way. Thus, the local sector bounds are preferred when formulating a tighter approximation of π_{DNN} , which yields the *largest* inner approximation of RoA¹ in the sense

¹ Based on the formulation of RoA (De Persis, Rotulo, & Tesi,

of robust control. We consider that each scalar activation function satisfies local sector-bounded restrictions, namely, $\varphi_i \in \text{Sec}[\rho_i, \sigma_i]$ holds around the equilibrium p_i^* with an input $p_i \in [\underline{p}_i, \bar{p}_i]$, $i \in \mathbb{N}_{[1, \ell]}$. The local sector bounds are aggregated into vectors $\rho, \sigma, \underline{p}, \bar{p}, p^* \in \mathbb{R}^a$, which yields the following quadratic constraint (Fazlyab, Morari, & Pappas, 2022).

Lemma 1 *The activation function φ satisfies the local sector bound $\text{Sec}[\rho, \sigma]$ around the point (p^*, m^*) for $p, p^* \in [\underline{p}, \bar{p}]$. Then, there exists $\gamma = \text{Col}(\gamma_1, \dots, \gamma_a)$ with $\gamma_i \geq 0$, such that*

$$\underbrace{\begin{bmatrix} \Delta p \\ \Delta m \end{bmatrix}^\top \begin{bmatrix} M_\sigma & -I_a \\ -M_\rho & I_a \end{bmatrix}^\top \begin{bmatrix} \mathbf{0}_a & M_\gamma \\ M_\gamma & \mathbf{0}_a \end{bmatrix} \begin{bmatrix} M_\sigma & -I_a \\ -M_\rho & I_a \end{bmatrix} \begin{bmatrix} \Delta p \\ \Delta m \end{bmatrix}}_{\triangleq \mathcal{M}_{\text{DNN}}} \geq 0 \quad (16)$$

holds for $m = \varphi(p)$, $\rho, \sigma, \underline{p}, \bar{p}, p^* \in \mathbb{R}^a$ with element-wise $\rho \leq \sigma$ and $\underline{p} \leq \bar{p}$, where $\Delta p \triangleq p - p^*$, $\Delta m \triangleq m - m^*$, and

$$M_\sigma \triangleq \text{Diag}(\sigma_1, \sigma_2, \dots, \sigma_a), M_\rho \triangleq \text{Diag}(\rho_1, \rho_2, \dots, \rho_a), \\ M_\gamma \triangleq \text{Diag}(\gamma_1, \gamma_2, \dots, \gamma_a). \quad (17)$$

Proof Based on the definitions of Δp and Δm , the offset local sector bound $\text{Sec}[\rho, \sigma]$ for the activation nonlinearity φ implies that there exist scalars $\gamma_i \geq 0, i \in \mathbb{N}_{[1, a]}$, which yields the condition $\gamma_i(\Delta m_i - \rho_i \Delta p_i)(\sigma_i \Delta p_i - \Delta m_i) \geq 0$. Then summing up this inequality from $i=1$ to $i=a$ leads to (16). The proof is along the same line as (Fazlyab, Morari, & Pappas, 2022), and more details are omitted.

Remark 3 *Before incorporating the quadratic constraint of π_{DNN} in (16) into the closed-loop stability analysis, leading to an inner approximation of robust RoA, we need to achieve the bounds $\underline{p}, \bar{p} \in \mathbb{R}^a$ of p , starting from the counterpart of the first layer $p_1 \in [\underline{p}_1, \bar{p}_1]$. Then, the bounds \underline{m}_1 and \bar{m}_1 can be derived by $m_1(k) = \varphi_1(p_1(k))$, hence to calculate the bounds $[\underline{p}_2, \bar{p}_2]$ of the preactivation p_2 . By the interval bound propagation (IBP) (Gowal, Dvijotham, Stanforth, Bunel, Qin, Uesato, Arandjelovic, Mann, & Kohli, 2018, Section 3), such calculation process is propagated through all layers of a trained π_{DNN} . More explicitly, the interval bounds on p_1 can be symmetrical about p_1^* with $\underline{p}_1 = 2p_1^* - \bar{p}_1$, which are taken into account in what follows.*

2023, Proposition 1), any Lyapunov-based sublevel set $\mathcal{E}_{P_1}^{\mathfrak{S}}(x^*) \triangleq \{x \in \mathbb{R}^n \mid \|x - x^*\|_{P_1}^2 \leq \mathfrak{S}\}$ contained in the region of $\mathcal{Z} \cup \{x^*\}$, with $\mathcal{Z} \triangleq \{x \in \mathbb{R}^n \mid \Delta \mathcal{V}(k) < 0\}$ and $\Delta \mathcal{V}(k)$ specified as Lemma 2, is a positive invariant set for the closed loop and implies an RoA estimation. Herein, the 1-level set $\mathcal{E}_{P_1}(x^*)$ with $\mathfrak{S}=1$ as (Hindi & Boyd, 1998) is considered as a metric for assessing stability, that is, the largest RoA inner approximation is in the sense of 1-level set. We make this statement to avoid readers' confusion.

We assume that the DNN controller is with zero-bias terms, such that the augmented state η can converge to the (local) equilibrium point η^* , which implies that the setpoint tracking error $\eta - \eta^*$ can converge to the original point. Within this context, zero bias in conjunction with $\mu(0) = 0$ can suit for the special case of $\bar{u}^* = \mathbf{0}_m$ and $\eta^* = \mathbf{0}_{\bar{n}}$, as discussed in (Yin, Seiler, Jin, & Arcak, 2022b, Assumption 1).

3.3 Closed-Loop Stability Analysis

For a sequence of time instants $\{\theta_{j,q}\}$, a function $H(\eta, k)$ mapping $\mathbb{R}^{\bar{n}} \times \mathbb{N}_{[\theta_{j,q}, \theta_{j+1,q}-1]}$ to \mathbb{R} is called a looped function, if $H(\eta(\theta_{j+1,q}), \theta_{j+1,q}) = H(\eta(\theta_{j,q}), \theta_{j,q})$ holds for $j \in \mathbb{N}_{[0, h(q)]}$. Based on the looped function defined in discrete time, the following lemma plays an important role in deriving the closed-loop stability guarantees in this subsection.

Lemma 2 *For scalars $\mu_1 < \mu_2$ with $\mu_1, \mu_2 \in \mathbb{R}_{>0}$, and a differentiable value function $V(\eta) : \mathbb{R}^{\bar{n}} \rightarrow \mathbb{R}_{\geq 0}$ for $\eta \in \mathbb{R}^{\bar{n}}$, satisfying $\mu_1 \|\eta\|_2^2 \leq V(\eta) \leq \mu_2 \|\eta\|_2^2$, the following two statements are equivalent.*

- (i) *The existence of looped function $H(\eta(k), k)$ ensures that $\Delta \mathcal{V}(k) \triangleq \mathcal{V}(k+1) - \mathcal{V}(k) < 0$ holds for $k \in [\theta_{j,q}, \theta_{j+1,q}-1]$, non-zero $\eta(\theta_{j,q})$ and $\{\theta_{j,q}\}$, where $\mathcal{V}(k) \triangleq V(\eta(k)) + H(\eta(k), k)$.*
- (ii) *The increment of $V(\eta)$ satisfies $\Delta V \triangleq V(\eta(\theta_{j+1,q})) - V(\eta(\theta_{j,q})) < 0$ with non-zero $\eta(\theta_{j,q})$ for a sequence $\{\theta_{j,q}\}$.*

Proof We sum up $\Delta \mathcal{V}(k)$ over the interval $[\theta_{j,q}, \theta_{j+1,q}-1]$ and take advantage of the definition of looped function as aforementioned. Allowing for $\Delta \mathcal{V}(k) < 0$ satisfying the first statement, we obtain

$$\sum_{k=\theta_{j,q}}^{\theta_{j+1,q}-1} \Delta \mathcal{V}(k) = \sum_{k=\theta_{j,q}}^{\theta_{j+1,q}-1} (V(\eta(k+1)) - V(\eta(k))) + \\ \sum_{k=\theta_{j,q}}^{\theta_{j+1,q}-1} (H(\eta(k+1), k+1) - H(\eta(k), k)) \\ = V(\eta(\theta_{j+1,q})) - V(\eta(\theta_{j,q})) = \Delta V < 0,$$

which can prove that the second statement holds.

In contrast, we suppose the second statement is satisfied and construct the looped function $H(\eta(k), k) = -V(\eta(k)) + k \Delta V / (\theta_{j+1,q} - \theta_{j,q})$ for $k \in [\theta_{j,q}, \theta_{j+1,q}-1]$, which satisfies $H(\eta(\theta_{j+1,q}), \theta_{j+1,q}) = H(\eta(\theta_{j,q}), \theta_{j,q})$. Hence, we calculate

$$\Delta \mathcal{V}(k) = (V(\eta(\theta_{j+1,q})) - V(\eta(\theta_{j,q})) / (\theta_{j+1,q} - \theta_{j,q})) < 0,$$

which can prove that the first statement holds.

Remark 4 *Lemma 2 provides a methodology of verifying the closed-loop stability of the event-triggered neural-feedback loops (5) based on a looped function $H(x(k), k)$, the value of which is not restricted to be positively definite, implying less conservatism of stability analysis. Within this context, the Lyapunov tracking loss $V(\eta)$ should only*

decrease at the communication instant k_q , rather than at each time instant k . Thus, the core of verifying closed-loop stability lies in selecting proper looped functions combined with the specified event-triggered logic, which motivates the following theorem.

Theorem 1 For specified scalars $1 \leq \vartheta_l < \vartheta_u$, $\epsilon_1, \epsilon_2 \in \mathbb{R}_{[0,1]}$, and $\mu, g \geq 0$ satisfying $1 - \mu - g^{-1} \geq 0$, the neural-feedback loops (5) asymptotically converge to the equilibrium point $(\eta^*, u^*, \omega^*, v^*, p^*, m^*)$ under the event-triggered communication scheme (13), where $\alpha(\theta_{j,q})$ converges to the origin with $\alpha(0) \geq 0$, if there exist matrices $P \succ 0$, $T_i \succ 0$, $\Xi_i \succ 0$, R, N_i , and a vector $\gamma \in \mathbb{R}^a$ with element-wise $\gamma_i \geq 0$ as decision variables, such that the following conditions

$$\begin{bmatrix} \mathcal{G} + \vartheta \Pi_i & \vartheta N_i \\ \star & -\vartheta T_i \end{bmatrix} \prec 0, \begin{bmatrix} (\bar{p}_{1,j} - p_{1,j}^*)^2 & [W_{1,j} \ \mathbf{0}_{1 \times \psi}] \\ \star & P \end{bmatrix} \succeq 0, (18)$$

hold for $\underline{p}_1 = 2p_1^* - \bar{p}_1$, $i \in \mathbb{N}_{[1,2]}$, $j \in \mathbb{N}_{[1,a_1]}$, $i \in \mathbb{N}_{[1,a]}$, and $\vartheta_l \leq \vartheta \leq \vartheta_u$, where $T_i \triangleq \text{Diag}(T_i, 3T_i)$,

$$\begin{aligned} \mathcal{G} &\triangleq (AL_1 + B\Sigma_1\Lambda_1)^\top P (AL_1 + B\Sigma_1\Lambda_1) + \mathcal{G}_1^\top (T_2 - T_1)\mathcal{G}_1 \\ &\quad + \mathcal{G}_2^\top M_\Theta \mathcal{G}_2 + \mathcal{G}_3^\top \mathcal{M}_{\text{DNN}} \mathcal{G}_3 + \text{Sym}(R_1^\top RR_2 - R_5^\top RR_6 \\ &\quad + N_1 R_9 + N_2 R_{10}) - L_1^\top PL_1 + \mathcal{Q}, \\ \mathcal{Q} &\triangleq \epsilon_1 L_4^\top \Xi_1 L_4 + \epsilon_2 L_8^\top \Xi_2 L_8 - (L_4 - L_8)^\top \Xi_2 (L_4 - L_8), \\ \Pi_1 &\triangleq \mathcal{G}_1^\top T_2 \mathcal{G}_1 + \text{Sym}(R_3^\top RR_7), \Pi_2 \triangleq \mathcal{G}_1^\top T_1 \mathcal{G}_1 + \text{Sym}(R_8^\top RR_4), \\ \Sigma_1 &\triangleq \text{Col}\left(\left[\Pi_{ux} \ \Pi_{um} \ \mathbf{0}_{m \times n}\right], \left[\mathbf{0}_{w \times n} \ \mathbf{0}_{w \times a} \ I_w\right]\right), \\ \Lambda_1 &\triangleq \text{Col}(L_8, L_2, L_3), \mathcal{G}_1 \triangleq \Lambda_2 AL_1 - \Lambda_2 L_1 + \Lambda_2 B\Sigma_1 \Lambda_1, \\ \mathcal{G}_2 &\triangleq CL_1 + D\Sigma_1 \Lambda_1, \mathcal{G}_3 \triangleq \text{Col}(\Pi_{px} L_8 + \Pi_{pm} L_2, L_2), \\ \Lambda_2 &\triangleq [I_n \ \mathbf{0}_{n \times \psi}], R_1 \triangleq \text{Col}(L_4, L_5, R_{1,3}, L_6 + R_{1,3}), \\ R_2 &\triangleq \text{Col}(-L_4, -L_5, R_{2,3}, L_7 - L_5 - \Lambda_2 L_1), \\ R_3 &\triangleq \text{Col}(L_4, L_5, \mathbf{0}_{n \times \bar{n}}, L_6), R_4 \triangleq \text{Col}(L_4, L_5, \mathbf{0}_{n \times \bar{n}}, L_7), \\ R_5 &\triangleq \text{Col}(\mathbf{0}_{n \times \bar{n}}, \mathbf{0}_{n \times \bar{n}}, \Lambda_2 L_1 - L_4, L_6 - L_4), R_7 \triangleq R_2 - R_6, \\ R_6 &\triangleq \text{Col}(\mathbf{0}_{n \times \bar{n}}, \mathbf{0}_{n \times \bar{n}}, L_5 - \Lambda_2 L_1, L_7 - L_5), R_8 \triangleq R_1 - R_5, \\ R_9 &\triangleq \text{Col}(\Lambda_2 L_1 - L_4, \Lambda_2 L_1 + L_4 - L_6), \bar{n} \triangleq z + a + w + 5n, \\ R_{10} &\triangleq \text{Col}(L_5 - \Lambda_2 L_1, L_5 + \Lambda_2 L_1 - L_7), L_1 \triangleq [I_z \ \mathbf{0}_{z \times (\bar{n} - z)}], \\ R_{1,3} &\triangleq \Lambda_2 AL_1 + \Lambda_2 B\Sigma_1 \Lambda_1 - L_4, L_2 \triangleq [\mathbf{0}_{a \times z} \ I_a \ \mathbf{0}_{a \times (\bar{n} - z - a)}], \\ R_{2,3} &\triangleq L_5 - \Lambda_2 AL_1 - \Lambda_2 B\Sigma_1 \Lambda_1, L_3 \triangleq [\mathbf{0}_{w \times (z+a)} \ I_w \ \mathbf{0}_{w \times 5n}], \\ L_j &\triangleq [\mathbf{0}_{n \times (z+a+w)} \ \mathbf{0}_{n \times (j-4)n} \ I_n \ \mathbf{0}_{n \times (8-j)n}], j \in \mathbb{N}_{[4,8]}. \end{aligned}$$

$W_{1,j}$ denotes the j -th row of the weight matrix W_1 . Then an ellipsoid $\mathcal{E}_{P_1}(x^*) \triangleq \{x \in \mathbb{R}^n \mid \|x - x^*\|_{P_1}^2 \leq 1\}$, where P_1 denotes the upper left block of P with the proper dimension, implies an inner approximation of RoA when $\alpha(0) = 0$.

Proof We recall the neural-feedback loops (5) and incorporate the dynamic variable $\alpha(\theta_{j,q})$ to the closed-loop stability

analysis. For $k \in [\theta_{j,q}, \theta_{j+1,q} - 1]$ with $j \in \mathbb{N}_{[0, h(q)]}$ and $q \in \mathbb{N}$, we select the value function with

$$\mathcal{W}(\eta(k), k) = V(\eta(k)) + H(\eta(k), k) + \alpha(k), \quad (19)$$

in which $V(\eta(k)) \triangleq \|\eta(k) - \eta^*\|_P^2$ with $p \succ 0$, $\alpha(k)$ in (12) is nonnegative in view of Remark 1. The looped function satisfies $H(\eta(k), k) \triangleq \sum_{\kappa=1}^3 H_\kappa(k)$ with the form

$$H_1(k) \triangleq 2\chi_1^\top(k) R \chi_2(k), \quad (20)$$

$$H_2(k) \triangleq (\theta_{j+1,q} - k) \left(\sum_{s=\theta_{j,q}}^k \|y(s)\|_{T_1}^2 - \|y(k)\|_{T_1}^2 \right), \quad (21)$$

$$H_3(k) \triangleq (k - \theta_{j,q}) \left(\|y(\theta_{j+1,q})\|_{T_2}^2 - \sum_{s=k}^{\theta_{j+1,q}} \|y(s)\|_{T_2}^2 \right), \quad (22)$$

where $R \in \mathbb{R}^{4n \times 4n}$, $T_i \succ 0$ with $i \in \mathbb{N}_{[1,2]}$, and

$$\begin{aligned} \chi_1 &\triangleq \text{Col}\left((k - \theta_{j,q})m_0, x_k - x_{\theta_{j,q}}, \sum_{s=\theta_{j,q}}^k x_s - x_{\theta_{j,q}}\right), \\ \chi_2 &\triangleq \text{Col}\left((\theta_{j+1,q} - k)m_0, x_{\theta_{j+1,q}} - x_k, \sum_{s=k}^{\theta_{j+1,q}} x_s - x_{\theta_{j+1,q}}\right), \\ m_0 &\triangleq \text{Col}(x_{\theta_{j,q}}, x_{\theta_{j+1,q}}), x_k \triangleq x(k) - x^*, x_{\theta_{j,q}} \triangleq x(\theta_{j,q}) - x^*, \\ x_s &\triangleq x(s) - x^*, x_{\theta_{j+1,q}} \triangleq x(\theta_{j+1,q}) - x^*, y(s) = x_{s+1} - x_s. \end{aligned}$$

Accordingly, the forward difference for each item in (19) can be calculated by $\Delta\alpha(k) = \alpha(k+1) - \alpha(k)$, and

$$\begin{aligned} \Delta V &= \zeta^\top(k) \left((AL_1 + B\Sigma_1\Lambda_1)^\top P (AL_1 + B\Sigma_1\Lambda_1) \right. \\ &\quad \left. - L_1^\top PL_1 \right) \zeta(k), \\ \Delta H_1 &= \zeta^\top(k) \text{Sym}(R_1^\top RR_2 - R_5^\top RR_6 + (k - \theta_{j,q})R_3^\top RR_7 \\ &\quad + (\theta_{j+1,q} - k)R_8^\top RR_4) \zeta(k), \\ \Delta H_2 &= (\theta_{j+1,q} - k - 1) \zeta^\top(k) \mathcal{G}_1^\top T_1 \mathcal{G}_1 \zeta(k) - \sum_{s=\theta_{j,q}}^{k-1} \|y(s)\|_{T_1}^2, \\ \Delta H_3 &= (k+1 - \theta_{j,q}) \zeta^\top(k) \mathcal{G}_1^\top T_2 \mathcal{G}_1 \zeta(k) - \sum_{s=k}^{\theta_{j+1,q}-1} \|y(s)\|_{T_2}^2 \end{aligned} \quad (23)$$

in which $\zeta(k) \triangleq \text{Col}(\eta_k, m_k, \omega_k, x_{\theta_{j,q}}, x_{\theta_{j+1,q}}, \sum_{s=\theta_{j,q}}^k x_s / (k - \theta_{j,q} + 1), \sum_{s=k}^{\theta_{j+1,q}} x_s / (\theta_{j+1,q} - k + 1), x_{k_q}) \in \mathbb{R}^{\bar{n}}$ with $\eta_k \triangleq \eta(k) - \eta^*$, $m_k \triangleq m(k) - m^*$, $\omega_k \triangleq \omega(k) - \omega^*$, and $x_{k_q} \triangleq x(k_q) - x^*$. By virtue of the nonlinearity isolation of π_{DNN} in (14), we have

$$\bar{u}(k) - \bar{u}^* = \Sigma_1 \text{Col}(x_{k_q}, m_k, \omega_k) = \Sigma_1 \Lambda_1 \zeta(k), \quad (24)$$

which is utilized for deriving ΔV in (23). Then, in the light of the summation inequality, we can further relax the summation terms of $\Delta H_2(k)$ and $\Delta H_3(k)$ by

$$\begin{aligned} -\sum_{s=\theta_{j,q}}^{k-1} \|y(s)\|_{T_1}^2 &\leq (k - \theta_{j,q}) \zeta^\top(k) N_1^\top T_1^{-1} N_1 \zeta(k) \\ &\quad + \zeta^\top(k) \text{Sym}(N_1 R_9) \zeta(k), \quad (25) \end{aligned}$$

$$\begin{aligned} -\sum_{s=k}^{\theta_{j+1,q}-1} \|y(s)\|_{T_2}^2 &\leq (\theta_{j+1,q} - k) \zeta^\top(k) N_2^\top T_2^{-1} N_2 \zeta(k) \\ &\quad + \zeta^\top(k) \text{Sym}(N_2 R_{10}) \zeta(k), \quad (26) \end{aligned}$$

with $\mathcal{T}_i \triangleq \text{Diag}(T_i, 3T_i)$. Recall the dynamic parameter $\alpha(\theta_{j,q})$ in (12) and its nonnegativity attribute, we can derive

$$\alpha(\theta_{j+1,q}) - \alpha(\theta_{j,q}) = -\mu\alpha(\theta_{j,q}) + \|\zeta(k)\|_{\mathcal{Q}}^2 \leq \|\zeta(k)\|_{\mathcal{Q}}^2. \quad (27)$$

Moreover, combining (14) with (16) leads to

$$\zeta^\top(k) \mathcal{G}_3^\top \mathcal{M}_{\text{DNN}} \mathcal{G}_3 \zeta(k) \geq 0. \quad (28)$$

Hence, by virtue of (4), (23), and (25)-(28) in conjunction with the Lyapunov function $\mathcal{W}(\eta(k), k)$ in (19), we obtain

$$\begin{aligned} & \Delta \mathcal{W}(\eta(k), k) + \alpha(\theta_{j+1,q}) - \alpha(\theta_{j,q}) - \Delta \alpha(k) \\ & + \|r(k) - r^*\|_{M_\Theta}^2 + \zeta^\top(k) \mathcal{G}_3^\top \mathcal{M}_{\text{DNN}} \mathcal{G}_3 \zeta(k) < 0, \end{aligned} \quad (29)$$

which implies that the following inequality

$$\begin{aligned} & \zeta^\top(k) \left(\mathcal{G} + \frac{k - \theta_{j,q}}{\vartheta} (\vartheta \Pi_1 + \vartheta N_1^\top \mathcal{T}_1^{-1} N_1) \right. \\ & \left. + \frac{\theta_{j+1,q} - k}{\vartheta} (\vartheta \Pi_2 + \vartheta N_2^\top \mathcal{T}_2^{-1} N_2) \right) \zeta(k) < 0, \end{aligned} \quad (30)$$

holds for $k \in [\theta_{j,q}, \theta_{j+1,q} - 1]$. For the coefficients $(k - \theta_{j,q})/\vartheta$ and $(\theta_{j+1,q} - k)/\vartheta$ belonging to $\mathbb{R}_{[0,1]}$, we can derive that $\mathcal{G} + \vartheta \Pi_i + \vartheta N_i^\top \mathcal{T}_i^{-1} N_i < 0$ holds for $i \in \mathbb{N}_{[1,2]}$. Hence, the first condition in (18) can be established by virtue of Schur complement, which is convex with regard to the decision variables. Note that the sixth term on the left side of (29) will be greater than zero, allowing for the local sector quadratic constraint (16). We then sum the remainder of (29) from $k = \theta_{j,q}$ to $\theta_{j+1,q} - 1$, which leads to

$$\begin{aligned} & \sum_{k=\theta_{j,q}}^{\theta_{j+1,q}-1} (\Delta \mathcal{W}(\eta(k), k) + \alpha(\theta_{j+1,q}) - \alpha(\theta_{j,q}) - \Delta \alpha(k)) \\ & + \sum_{k=\theta_{j,q}}^{\theta_{j+1,q}-1} \|r(k) - r^*\|_{M_\Theta}^2 \\ & = V(\eta(\theta_{j+1,q})) + (\vartheta - 1)\alpha(\theta_{j+1,q}) - V(\eta(\theta_{j,q})) - (\vartheta - 1)\alpha(\theta_{j,q}) \\ & + \sum_{k=\theta_{j,q}}^{\theta_{j+1,q}-1} \|r(k) - r^*\|_{M_\Theta}^2 \leq -\bar{h}_1 \|\zeta(\theta_{j,q})\|^2 < 0, \end{aligned} \quad (31)$$

holding for the constant sampling interval $\vartheta \in \mathbb{N}_{[\vartheta_l, \vartheta_u]}$ and the looped function $H(x(\theta_{j+1,q}), \theta_{j+1,q}) = H(x(\theta_{j,q}), \theta_{j,q})$. We generalize the time interval from $[\theta_{j,q}, \theta_{j+1,q} - 1]$ to $[0, k_{\mathbb{N}}]$ with $\mathbb{N} \in \mathbb{N}_{>1}$. Let $k_0 = 0$ and recap $\theta_{h(q)+1,q} = k_q + \vartheta(h(q) + 1) = k_{q+1}$, based on the existence of $\bar{h}_1 \in \mathbb{R}_{>0}$ in (31), we further obtain

$$\begin{aligned} & \sum_{q=0}^{\mathbb{N}-1} \sum_{j=0}^{h(q)} (V(\eta(\theta_{j+1,q})) + (\vartheta - 1)\alpha(\theta_{j+1,q}) - V(\eta(\theta_{j,q})) \\ & - (\vartheta - 1)\alpha(\theta_{j,q}) + \sum_{k=\theta_{j,q}}^{\theta_{j+1,q}-1} \|r(k) - r^*\|_{M_\Theta}^2) \\ & = V(\eta(k_{\mathbb{N}})) + (\vartheta - 1)\alpha(\theta_{k_{\mathbb{N}}}) - V(\eta(0)) - (\vartheta - 1)\alpha(0) \\ & + \sum_{q=0}^{\mathbb{N}-1} \sum_{j=0}^{h(q)} \sum_{k=\theta_{j,q}}^{\theta_{j+1,q}-1} \|r(k) - r^*\|_{M_\Theta}^2 \end{aligned} \quad (32)$$

$$\leq -\sum_{q=0}^{\mathbb{N}-1} \sum_{j=0}^{h(q)} \bar{h}_1 \|\zeta(\theta_{j,q})\|^2. \quad (33)$$

Note that the last term of (32) equals to $\sum_{k=0}^{k_{\mathbb{N}}} \|r(k) - r^*\|_{M_\Theta}^2$, which is no less than zero, allowing for the definition of IQC

in (4). By virtue of (32) and (33), we obtain

$$\begin{aligned} & V(\eta(k_{\mathbb{N}})) + (\vartheta - 1)\alpha(\theta_{k_{\mathbb{N}}}) - V(\eta(0)) - (\vartheta - 1)\alpha(0) \\ & \leq -\sum_{k=0}^{k_{\mathbb{N}}} \bar{h}_1 \|\zeta(k)\|^2, \end{aligned} \quad (34)$$

where the last term equals to the counterpart of (33). Hence, the asymptotical stability of $V(\eta(k)) + (\vartheta - 1)\alpha(k)$ is ensured, that is, $\eta(k)$ and $\alpha(k)$ converge to η^* and the origin, respectively, as k tends to ∞ . Besides, the second inequality of (18) validates the prerequisite of local quadratic constraint of π_{DNN} (16). We intuitively obtain $W_{1,j} P_1^{-1} W_{1,j}^\top \leq (\bar{p}_{1,j} - p_{1,j}^*)^2$, $j \in \mathbb{N}_{[1,a_1]}$ by utilizing Schur complement, which ensures that the sublevel set $\mathcal{E}_{P_1}(x^*)$ is contained in the set $\mathcal{R} \triangleq \{x \in \mathbb{R}^n \mid \|W_1(x - x^*)\|^2 \leq (\bar{p}_1 - p_1^*)\}$ in view of the constrained quadratic (Hindi & Boyd, 1998, Lemma 1) combined with the IBP technique. Thus, $p_1 \in [\underline{p}_1, \bar{p}_1]$ holds if $x(k) \in \mathcal{E}_{P_1}(x^*)$, and the local property is reasonable for the event-triggered π_{DNN} .

Recalling $\vartheta \geq 1$ and the nonnegativity of $\alpha(k_q)$ in the event-triggered scheme (13) and letting $\alpha(0) = 0$ as specified in (12), the inequality (34) leads to $V(\eta(k_{\mathbb{N}})) - V(\eta(0)) \leq -\sum_{k=0}^{k_{\mathbb{N}}} \bar{h}_1 \|\zeta(k) - \zeta^*\|^2$, which implies that $\eta(k) \in \mathcal{E}_P(\eta^*) \triangleq \{\eta \in \mathbb{R}^n \mid \|\eta - \eta^*\|_P^2 \leq 1\}$ holds for $\eta(0) \in \mathcal{E}_P(\eta^*)$. In view of the initial value $\xi(0) = 0$ of virtual filter (3), we obtain that $\eta(0) \in \mathcal{E}_P(\eta^*)$ yields $x(0) \in \mathcal{E}_{P_1}(x^*)$, acting as an inner approximation of robust RoA defined by (6), where P_1 denotes the upper left block of P . The proof is completed.

The feasible solution of (18) captures an inner approximation of robust RoA in (6), since the volume of $\mathcal{E}_{P_1}(x^*)$ is proportional to the determinant of P_1 , described by $\text{Det}(P_1)$ (Hindi & Boyd, 1998, Subsection 2.1). For computing the largest inner approximation of robust RoA, we can formulate the following optimization problem

$$\min_{P > 0, T_i > 0, \Xi_i > 0, \gamma \geq 0, R, N_i} \log(\text{Det}(P_1)), \text{ s.t. (18) holds,} \quad (35)$$

which is convex about all decision variables defined in Theorem 1.

Remark 5 Note that a particular uncertainty Θ implies the existence of a class of time-domain IQCs depicted by a virtual filter Φ_Θ in conjunction with a weight matrix M_Θ , extracting from the constraint set \mathcal{M}_Θ with $M_\Theta \in \mathcal{M}_\Theta \subseteq \mathbb{S}^\kappa$. Therefore, the convex optimization (35) can also regard M_Θ as an additional decision variable, leading to less conservatism about calculating the triggering parameters of (11), compared to the scenario of fixed M_Θ , which covers more flexibility of stability analysis by LMIs in the sense of IQCs (Lessard, Recht, & Packard, 2016, Subsection 3.2). Moreover, the upper bound \bar{p}_1 of the first-layer preactivation of π_{DNN} (7) affects the size of inner approximation of robust RoA explicitly. The local sector bound $\text{Sec}[\rho, \sigma]$ is sharpened by decreasing the value of $\bar{p}_1 - p_1^*$, which improves the robust RoA approximation in terms of reducing the convex relaxation error of π_{DNN} . However, it narrows the size of con-

strained set \mathcal{R} as discussed in Appendix A, which contains the ellipsoid $\mathcal{E}_{P_1}(x^*)$ (Hindi & Boyd, 1998, Lemma 1), hence to affect RoA inner approximations. In contrast, enlarging $\bar{p}_1 - p_1^*$ yields a larger constrained set \mathcal{R} containing $\mathcal{E}_{P_1}(x^*)$ and implies a looser local sector bound $\text{Sec}[\rho, \sigma]$. For further reducing conservatism, we can parameterize $\bar{p}_1 - p_1^* = \varsigma \mathbf{1}_{a_1}$ with $\underline{\varsigma} \leq \varsigma \leq \bar{\varsigma}$, in which $\bar{\varsigma}$ is the largest value preserving the feasibility of condition (18). Hence, assessing ς within the gridded interval $[\underline{\varsigma}, \bar{\varsigma}]$ leads to the largest inner approximation of robust RoA. Additionally, different from the time-triggered scheme (Yin, Seiler, & Arca, 2022a), the interval ϑ of event-triggered logic (13) also affects the RoA estimation. Large ϑ is beneficial for reducing computation burden, but the value of ϑ (or ϑ_u) is correlated to the feasible solution of (35). Within this context, the largest inner approximation of robust RoA is captured by adjusting ϑ through $[\vartheta_l, \vartheta_u]$, which yields a tradeoff between the communication burden and the stability metric. We can synthesize the best event-triggered neural control policy (9) by achieving the largest RoA approximation.

Remark 6 We make the discussions about the novelty and comparison of Theorem 1 in what follows, since fewer results have concentrated on the event-triggered neural control design problems. First, the convex optimization (35) incorporates the event-triggered transmission (13) into the neural-feedback loops (5) for assessing the stability metric by robust RoA estimation. Remark 5 leads to the best event-triggered logic corresponding to the largest inner approximation of robust RoA, which builds upon the strict stability criterion (18), such that both the better adaptivity to uncertainty impacts by virtue of π_{DNN} and the more efficient communication transmission induced by event-triggered logic can be achieved synchronously. Second, albeit the Lipschitz continuity assumption on π_{DNN} (Jin & Lavaei, 2018, Lemma 4.2) can lead to its quadratic constraint, associated with the forward dynamics of closed-loop system (Talukder & Kumar, 2023, Proposition 1), to support stability analysis, the identification of Lipschitz bound also needs an extra calculation step, such as the LipSDP procedure (Fazlyab, Robey, Hassani, Morari, & Pappas, 2019, Theorem 2) and the maximum absolute row sum approach (Talukder & Kumar, 2023, Equation (16)), which can increase computation burden especially for a large-scale π_{DNN} . As an alternative, the local sector-bounded attribute of nonlinear activation function φ can represent the quadratic constraint of π_{DNN} , and the nonlinear isolation technique (14) can integrate the activation m_i of each layer of π_{DNN} into an augmented vector ζ to perform stability analysis of ETC systems. Moreover, the dimensions of decision variables in Theorem 1 are distinctly less than the counterparts calculated by Kronecker product (Talukder & Kumar, 2023), which also reduces computation burden. Third, the stability verification performed in Theorem 1 relies on auxiliary looped functions, which implies less conservatism as shown in Remark 4. Recalling the theoretical derivations as aforementioned, the condition $H(\theta_{j+1,q}) = H(\theta_{j,q}) = 0$ holds. Compared to the results for linear systems (Seuret, 2012; Wang, Berberich, Sun, Wang, Allgöwer, & Chen, 2023), the nonlinearity of π_{DNN} herein is

relaxed to develop stability criterion in the sense of convex optimization, which generalizes the methods to the scenario of nonlinear systems and provides strict theoretical guarantees in the complete time domain based on the IQC of uncertainty impact and the summation inequality.

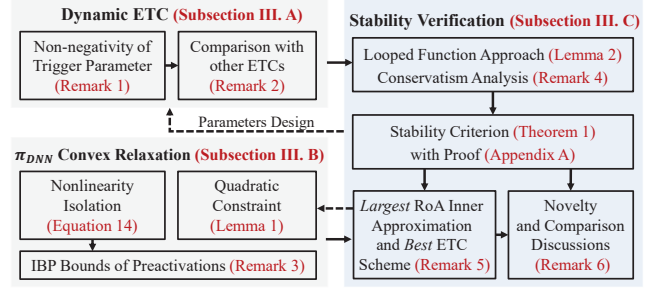


Fig. 2. The architecture of event-triggered neural control in Section 3.

4 Self-Triggered Neural Control Policy

4.1 Self-Triggered Scheme

The core of self-triggered communication transmission lies in specifying a function $\mathcal{U}(x(k_q))$ to determine the next transmission instant k_{q+1} , namely,

$$k_{q+1} = k_q + \mathcal{U}(x(k_q), s_k), \quad (36)$$

where $s_k = k_{q+1} - k_q$ with $s_k \in \mathbb{N}_{[1, \bar{s}]}$, $\bar{s} \in \mathbb{N}_{>1}$. Different from event-triggered schemes using the current sampled data, self-triggered schemes depend on a predicted state $x(k_q + s_k)$ to determine the next transmission instant. For specifying the term $\mathcal{U}(x(k_q), s_k)$ in (36), we deploy the following condition

$$\check{\epsilon}_1 \|x(k_q + s_k) - x^*\|_{\check{\Xi}_1}^2 + \check{\epsilon}_2 \|x(k_q) - x^*\|_{\check{\Xi}_1}^2 - \|e(s_k)\|_{\check{\Xi}}^2 \geq 0, \quad (37)$$

where $\check{\epsilon}_1, \check{\epsilon}_2 \in \mathbb{R}_{[0,1]}$ are discount parameters, $\check{\Xi}_1, \check{\Xi}_2 \in \mathbb{S}_{>0}^n$ are weight matrices, and the divergence between $x(k_q)$ at the latest transmission instant k_q and $x(k_q + s_k)$ at the predicted time instant $k_q + s_k$ can be defined by $e(s_k) \triangleq x(k_q + s_k) - x(k_q)$. Hence, the condition (37) is recapped by

$$\mathcal{S}(x(k_q), s_k) = \begin{bmatrix} x(k_q + s_k) - x^* \\ x(k_q) - x^* \end{bmatrix}^\top \begin{bmatrix} \check{\epsilon}_1 \check{\Xi}_1 - \check{\Xi}_2 & \check{\Xi}_2 \\ \star & \check{\epsilon}_2 \check{\Xi}_1 - \check{\Xi}_2 \end{bmatrix} \times \begin{bmatrix} x(k_q + s_k) - x^* \\ x(k_q) - x^* \end{bmatrix} \geq 0. \quad (38)$$

The time instant $k_q + s_k$ reveals the next transmission on the premise of $\mathcal{S}(x(k_q), s_k) \geq 0$. The ZOH is utilized to maintain the sampled state $x(k_q + s_k)$ within $[k_{q+1}, k_{q+2} - 1]$, when it is transmitted to the controller π_{DNN} . Meanwhile, the self-triggered scheme is used to determine the next transmission

time instant k_{q+2} . The term $\mathcal{U}(x(k_q), s_k)$ is with the form

$$\mathcal{U}(x(k_q), s_k) = \max_{s_k \in \mathbb{N}} \{s_k \in \mathbb{N}_{\geq 1} | \mathcal{S}(x(k_q), s_k) \geq 0\}. \quad (39)$$

Hence, in view of the self-triggered scheme, the next transmission time instant k_{q+1} is predicted by the current measurement at time instant k_q , such that continuous monitoring of system state is unnecessary.

Remark 7 The static self-triggered scheme (36)-(39) is akin to the results (Wan, Luan, Karimi, & Liu, 2021; Wang, Berberich, Sun, Wang, Allgöwer, & Chen, 2023; Wildhagen, Berberich, Hertneck, & Allgöwer, 2023). Here, we only state the comparisons and discussions. First, compared to (Wang, Berberich, Sun, Wang, Allgöwer, & Chen, 2023, Subsection IV.A), the lifting technique is unsuitable for the system (5) with nonlinear π_{DNN} , while the deployment of ZOH and the pretrained controller can still lead to $x(k_q + s_k)$ based on (9), and the extension of (Wildhagen, Berberich, Hertneck, & Allgöwer, 2023) to the nonlinear situation is promising. Second, the self-triggered policy (Wan, Luan, Karimi, & Liu, 2021, Theorem 1) depends heavily on convex relaxations to build the correlations between $x(k_q)$ and $x(k)$, whereas, the comparison lemma is unavailable for the discrete-time scenario directly. Note that the self-triggered condition (38) implies less conservatism and more conciseness, since an intermediate variable $x(k)$ is excluded intuitively. Moreover, different from (Cao, Niu, & Zou, 2023, Subsection 2.2), the network-induced delay during the state transmission is not incorporated into the self-triggered scheme as aforementioned, but it leaves the room for future research. Third, compared to the event-triggered scheme in the Subsection 3.1, the event-based condition (13) boils down to the self-triggered one (37) by letting $\alpha=0$, $g=1$, and $j\vartheta=s_k$, while both of them depends on the current transmission $x(k_q)$.

We shall perform the closed-loop stability verification of the self-triggered neural-feedback loops (5) and (9), allowing for the self-triggered strategy in Subsection 4.1 and the convex relaxation of π_{DNN} in Subsection 3.2, in what follows.

4.2 Closed-Loop Stability Analysis

We search for a looped function $\bar{W}(\eta, k) : \mathbb{R}^{\bar{n}} \times \mathbb{N}_{[k_q, k_{q+1}-1]} \rightarrow \mathbb{R}$, such that $\bar{W}(\eta(k_{q+1}), k_{q+1}) = \bar{W}(\eta(k_q), k_q)$ holds for $s_k \in \mathbb{N}_{[1, \bar{s}]}$. Based on the quadratic constraint (16) and the nonlinearity isolation (14) of π_{DNN} , we perform the controller-dynamic association for closed-loop stability analysis under the self-triggered scheme (36) and (39). The following lemma provides a tool for stability analysis using a looped function for the scenario of self-triggered scheme.

Lemma 3 For scalars $\check{\mu}_1 < \check{\mu}_2$ with $\check{\mu}_1, \check{\mu}_2 \in \mathbb{R}_{>0}$, and a differentiable value function $\bar{V}(\eta) : \mathbb{R}^S \rightarrow \mathbb{R}_{\geq 0}$ for $\eta \in \mathbb{R}^S$, satisfying $\check{\mu}_1 \|\eta\|_2^2 \leq \bar{V}(\eta) \leq \check{\mu}_2 \|\eta\|_2^2$, the following two statements are equivalent.

(i) The existence of looped function \bar{W} ensures that $\Delta \bar{V}(k) \triangleq$

$\bar{V}(k+1) - \bar{V}(k) < 0$ holds for $k \in [k_q, k_{q+1}-1]$, non-zero $\eta(k_q)$ and $\{k_q\}$, where $\bar{V}(k) \triangleq \bar{V}(\eta(k)) + \bar{W}(\eta(k), k)$.

(ii) The increment $\Delta \bar{V} \triangleq \bar{V}(\eta(k_{q+1})) - \bar{V}(\eta(k_q)) < 0$ holds with $\eta(k_q) \neq 0$ for a sequence $\{k_q\}$.

Proof The proof is similar to the counterpart of Lemma 2, and we omit it here due to the limited space.

Theorem 2 For specified scalars $\check{\epsilon}_1, \check{\epsilon}_2 \in \mathbb{R}_{[0,1]}$ and a positive integer $\bar{s} > 1$, the neural-feedback loops (5) asymptotically converge to the equilibrium point $(\eta^*, u^*, \omega^*, \nu^*, p^*, m^*)$ under the self-triggered communication scheme (36) and (39), if there exist matrices $\bar{P} \succ 0$, $\bar{T}_i \succ 0$, $\check{\Xi}_i \succ 0$, \bar{R}, \bar{N} , a vector $\gamma \in \mathbb{R}^a$ with element-wise $\gamma_i \geq 0$, and scalars $\bar{\lambda}_i > 0$ as the decision variables, such that the conditions

$$\begin{bmatrix} \bar{\mathcal{G}} & \bar{\partial}_1(\bar{N}_i, \bar{R}) \\ \star & -\bar{\partial}_2(\bar{T}_i, \bar{\lambda}_i) \end{bmatrix} \prec 0, \begin{bmatrix} (\bar{p}_{1,j} - \bar{p}_{1,j}^*)^2 [W_{1,j} \mathbf{0}_{1 \times \psi}] \\ \star & \bar{P} \end{bmatrix} \succeq 0, \quad (40)$$

hold for $\bar{p}_1 = -\bar{p}_1$, $i \in \mathbb{N}_{[1,2]}$, $j \in \mathbb{N}_{[1,a]}$, and $i \in \mathbb{N}_{[1,a]}$, where $\bar{T}_i \triangleq \text{Diag}(\bar{T}_i, 3\bar{T}_i)$,

$$\begin{aligned} \bar{\mathcal{G}} &\triangleq (A\bar{L}_1 + B\Sigma_1\bar{\Lambda}_1)^\top \bar{P} (A\bar{L}_1 + B\Sigma_1\bar{\Lambda}_1) + (\bar{s}-1)\bar{\mathcal{G}}_1^\top \bar{T}_1 \bar{\mathcal{G}}_1 + \\ &(\bar{s}+1)\bar{\mathcal{G}}_1^\top \bar{T}_2 \bar{\mathcal{G}}_1 + \bar{s}\bar{\lambda}_1 \bar{R}_7^\top \bar{R}_7 + \bar{s}\bar{\lambda}_2 \bar{R}_4^\top \bar{R}_4 + \bar{\mathcal{G}}_2^\top M_{\Theta} \bar{\mathcal{G}}_2 + \\ &\bar{\mathcal{G}}_3^\top \mathcal{M}_{\text{DNN}} \bar{\mathcal{G}}_3 + \text{Sym}(\bar{R}_1^\top \bar{R}_2 - \bar{R}_5^\top \bar{R}_6 + \bar{N}_1 \bar{R}_9 + \bar{N}_2 \bar{R}_{10}) \\ &- \bar{R}_{11}^\top \check{\Xi} \bar{R}_{11} - \bar{L}_1^\top \bar{P} \bar{L}_1, \\ \bar{\partial}_1 &\triangleq [\bar{s}\bar{N}_1 \quad \bar{s}\bar{N}_2 \quad \bar{s}\bar{R}_3^\top \bar{R} \quad \bar{s}\bar{R}_8^\top \bar{R}], \bar{\mathcal{G}}_2 \triangleq C\bar{L}_1 + D\Sigma_1\bar{\Lambda}_1, \\ \bar{\partial}_2 &\triangleq \text{Diag}(\bar{s}\bar{T}_1, \bar{s}\bar{T}_2, \bar{s}\bar{\lambda}_1 I_{4n}, \bar{s}\bar{\lambda}_2 I_{4n}), \bar{R}_7 \triangleq \bar{R}_2 - \bar{R}_6, \\ \bar{\mathcal{G}}_1 &\triangleq \Lambda_2 A\bar{L}_1 - \Lambda_2 \bar{L}_1 + \Lambda_2 B\Sigma_1\bar{\Lambda}_1, \bar{\Upsilon}_3 \triangleq \text{Col}(\bar{L}_4, \bar{L}_5, \mathbf{0}_{n \times \bar{n}}, \bar{L}_6), \\ \bar{\mathcal{G}}_3 &\triangleq \text{Col}(\Pi_{px} \bar{L}_4 + \Pi_{pm} \bar{L}_2, \bar{L}_2), \bar{\Upsilon}_4 \triangleq \text{Col}(\bar{L}_4, \bar{L}_5, \mathbf{0}_{n \times \bar{n}}, \bar{L}_7), \\ \bar{R}_1 &\triangleq \text{Col}(\bar{L}_4, \bar{L}_5, \bar{R}_{12}, \bar{L}_6 + \bar{R}_{12}), \bar{R}_8 \triangleq \bar{R}_1 - \bar{R}_5, \\ \bar{R}_2 &\triangleq \text{Col}(-\bar{L}_4, -\bar{L}_5, \bar{R}_{13}, \bar{L}_7 - \bar{L}_5 - \Lambda_2 \bar{L}_1), \bar{R}_{11} \triangleq \text{Col}(\bar{L}_5, \bar{L}_4), \\ \bar{R}_5 &\triangleq \text{Col}(\mathbf{0}_{n \times \bar{n}}, \mathbf{0}_{n \times \bar{n}}, \Lambda_2 \bar{L}_1 - \bar{L}_4, \bar{L}_6 - \bar{L}_4), \bar{L}_1 \triangleq [I_z \quad \mathbf{0}_{z \times (\bar{n}-z)}], \\ \bar{R}_6 &\triangleq \text{Col}(\mathbf{0}_{n \times \bar{n}}, \mathbf{0}_{n \times \bar{n}}, \bar{L}_5 - \Lambda_2 \bar{L}_1, \bar{L}_7 - \bar{L}_5), \check{\Xi} \triangleq [\mathcal{X}_1 \quad \mathcal{X}_2], \\ \bar{R}_9 &\triangleq \text{Col}(\Lambda_2 \bar{L}_1 - \bar{L}_4, \Lambda_2 \bar{L}_1 + \bar{L}_4 - \bar{L}_6), \bar{n} \triangleq z + a + w + 4n, \\ \bar{R}_{10} &\triangleq \text{Col}(\bar{L}_5 - \Lambda_2 \bar{L}_1, \bar{L}_5 + \Lambda_2 \bar{L}_1 - \bar{L}_7), \bar{\Lambda}_1 \triangleq \text{Col}(\bar{L}_4, \bar{L}_2, \bar{L}_3), \\ \bar{R}_{12} &\triangleq \Lambda_2 A\bar{L}_1 + \Lambda_2 B\Sigma_1\bar{\Lambda}_1, \bar{R}_{13} \triangleq \bar{L}_5 - \Lambda_2 A\bar{L}_1 - \Lambda_2 B\Sigma_1\bar{\Lambda}_1, \\ \bar{L}_2 &\triangleq [\mathbf{0}_{a \times z} \quad I_a \quad \mathbf{0}_{a \times (\bar{n}-z-a)}], \bar{L}_3 \triangleq [\mathbf{0}_{w \times (z+a)} \quad I_w \quad \mathbf{0}_{w \times 4n}], \\ \bar{L}_j &\triangleq [\mathbf{0}_{n \times (z+a+w)} \quad \mathbf{0}_{n \times (j-4)n} \quad I_n \quad \mathbf{0}_{n \times (\tau-j)n}], j \in \mathbb{N}_{[4,7]}, \\ \mathcal{X}_1 &\triangleq \text{Col}(\check{\epsilon}_1 \check{\Xi}_1 - \check{\Xi}_2, \check{\Xi}_2^\top), \mathcal{X}_2 \triangleq \text{Col}(\check{\Xi}_2, \check{\epsilon}_2 \check{\Xi}_1 - \check{\Xi}_2), \end{aligned}$$

and the other terms embedded in (40) are consistent to the counterparts in Theorem 1, Then the ellipsoid $\mathcal{E}_{\bar{P}_1}(x^*)$, where \bar{P}_1 is the upper left block of \bar{P} with the proper dimension, implies an inner approximation of RoA.

Proof We recall the neural-feedback loops (5) with an augmented state $\eta(k)$, and incorporate the self-triggered trans-

mission scheme (36) and (39) to the closed-loop stability analysis. For $k \in [k_q, k_{q+1}-1]$ with $s_k = k_{q+1} - k_q$ and $s_k \in \mathbb{N}_{[1, \bar{s}]}$, we select a value function with the form

$$\bar{V}(\eta(k), k) = \bar{V}(\eta(k)) + \bar{W}(\eta(k), k), \quad (41)$$

where $\bar{V}(\eta(k)) = \|\eta(k) - \eta^*\|_{\bar{P}}^2$ with $\bar{P} \succ 0$, and $\bar{W}(\eta(k), k)$ is a looped function $\bar{W}(\eta(k), k) \triangleq \sum_{\kappa=1}^3 \bar{W}_\kappa(k)$ with

$$\bar{W}_1(k) \triangleq 2\bar{\chi}_1^\top(k) \bar{R} \bar{\chi}_2(k), \quad (42)$$

$$\bar{W}_2(k) \triangleq (k_{q+1} - k) \left(\sum_{s=k_q}^k \|y(s)\|_{\bar{T}_1}^2 - \|y(k)\|_{\bar{T}_1}^2 \right), \quad (43)$$

$$\bar{W}_3(k) \triangleq (k - k_q) \left(\|y(k_{q+1})\|_{\bar{T}_2}^2 - \sum_{s=k}^{k_{q+1}} \|y(s)\|_{\bar{T}_2}^2 \right), \quad (44)$$

where $\bar{R} \in \mathbb{R}^{4n \times 4n}$, $\bar{T}_i \succ 0$ with $i \in \mathbb{N}_{[1, 2]}$, and

$$\bar{\chi}_1 \triangleq \text{Col} \left((k - k_q) \bar{m}_0, x_k - x_{k_q}, \sum_{s=k_q}^k x_s - x_{k_q} \right),$$

$$\bar{\chi}_2 \triangleq \text{Col} \left((k_{q+1} - k) m_0, x_{k_{q+1}} - x_k, \sum_{s=k}^{k_{q+1}} x_s - x_{k_{q+1}} \right),$$

$$m_0 \triangleq \text{Col}(x_{k_q}, x_{k_{q+1}}), x_k \triangleq x(k) - x^*, x_{k_q} \triangleq x(k_q) - x^*,$$

$$x_s \triangleq x(s) - x^*, x_{k_{q+1}} \triangleq x(k_{q+1}) - x^*, y(s) = x_{s+1} - x_s.$$

Accordingly, the forward difference for each item in (41) can be calculated by

$$\begin{aligned} \Delta \bar{V} &= \bar{\zeta}^\top(k) \left((A\bar{L}_1 + B\Sigma_1 \bar{\Lambda}_1)^\top \bar{P} (A\bar{L}_1 + B\Sigma_1 \bar{\Lambda}_1) \right. \\ &\quad \left. - \bar{L}_1^\top \bar{P} \bar{L}_1 \right) \bar{\zeta}(k), \\ \Delta \bar{W}_1 &= \bar{\zeta}^\top(k) \text{Sym}(\bar{R}_1^\top \bar{R} \bar{R}_2 - \bar{R}_1^\top \bar{R} \bar{R}_6 + (k - k_q) \bar{R}_3^\top \bar{R} \bar{R}_7 \\ &\quad + (k_{q+1} - k) \bar{R}_8^\top \bar{R} \bar{R}_4) \bar{\zeta}(k), \\ \Delta \bar{W}_2 &= (k_{q+1} - k - 1) \bar{\zeta}^\top(k) \bar{\mathcal{G}}_1^\top \bar{T}_1 \bar{\mathcal{G}}_1 \bar{\zeta}(k) - \sum_{s=k_q}^{k-1} \|y(s)\|_{\bar{T}_1}^2, \\ \Delta \bar{W}_3 &= (k + 1 - k_q) \bar{\zeta}^\top(k) \bar{\mathcal{G}}_1^\top \bar{T}_2 \bar{\mathcal{G}}_1 \bar{\zeta}(k) - \sum_{s=k}^{k_{q+1}-1} \|y(s)\|_{\bar{T}_2}^2, \end{aligned} \quad (45)$$

in which $\bar{\zeta}(k) \triangleq \text{Col}(\eta_k, m_k, \omega_k, x_{k_q}, x_{k_{q+1}}, \sum_{s=k_q}^k x_s / (k - k_q + 1), \sum_{s=k}^{k_{q+1}} x_s / (k_{q+1} - k + 1)) \in \mathbb{R}^{\bar{n}}$, with $\eta_k, m_k, \omega_k, x_{k_q}$ prescribed as in (23) and $x_{k_{q+1}} \triangleq x(k_{q+1}) - x^*$. By virtue of the nonlinearity isolation of π_{DNN} in (14), we have

$$\bar{u}(k) - \bar{u}^* = \Sigma_1 \text{Col}(x_{k_q}, m_k, \omega_k) = \Sigma_1 \bar{\Lambda}_1 \bar{\zeta}(k), \quad (46)$$

which is utilized for deriving $\Delta \bar{V}$ in (45). Then, in the light of the summation inequality (Chen, Xu, Jia, & Zhang, 2016, Corollary 3), we can further relax the summation terms of $\Delta \bar{W}_2(k)$ and $\Delta \bar{W}_3(k)$ by

$$-\sum_{s=k_q}^{k-1} \|y(s)\|_{\bar{T}_1}^2 \leq (k - k_q) \bar{\zeta}^\top(k) \bar{N}_1^\top \bar{T}_1^{-1} \bar{N}_1 \bar{\zeta}(k) + \bar{\zeta}^\top(k) \text{Sym}(\bar{N}_1 \bar{R}_9) \bar{\zeta}(k), \quad (47)$$

$$-\sum_{s=k}^{k_{q+1}-1} \|y(s)\|_{\bar{T}_2}^2 \leq (k_{q+1} - k) \bar{\zeta}^\top(k) \bar{N}_2^\top \bar{T}_2^{-1} \bar{N}_2 \bar{\zeta}(k) + \bar{\zeta}^\top(k) \text{Sym}(\bar{N}_2 \bar{R}_{10}) \bar{\zeta}(k), \quad (48)$$

with $\bar{T}_i \triangleq \text{Diag}(\bar{T}_i, 3\bar{T}_i)$. Moreover, combining (14) with (16) for the convex relaxation of π_{DNN} leads to

$$\bar{\zeta}^\top(k) \bar{\mathcal{G}}_3^\top \mathcal{M}_{\text{DNN}} \bar{\mathcal{G}}_3 \bar{\zeta}(k) \geq 0. \quad (49)$$

Hence, by virtue of (4), (45), and (47)-(49) combined with the self-triggered scheme (36) and (39), we obtain

$$\begin{aligned} \Delta \bar{V}(\eta(k), k) + \|r(k) - r^*\|_{M_\Theta}^2 + \bar{\zeta}^\top(k) \bar{\mathcal{G}}_3^\top \mathcal{M}_{\text{DNN}} \bar{\mathcal{G}}_3 \bar{\zeta}(k) \\ - \mathcal{S}(x(k_q), s_k) < 0, \end{aligned} \quad (50)$$

holding for $k \in [k_q, k_{q+1}-1]$, which implies that

$$\begin{aligned} \bar{\zeta}^\top(k) \left(\bar{\mathcal{G}} + (k - k_q) \bar{\Pi}_1 + (k_{q+1} - k) \bar{\Pi}_2 + (k - k_q) \bar{N}_1^\top \bar{T}_1^{-1} \bar{N}_1 \right. \\ \left. + (k_{q+1} - k) \bar{N}_2^\top \bar{T}_2^{-1} \bar{N}_2 \right) \bar{\zeta}(k) < 0, \end{aligned} \quad (51)$$

is satisfied with the terms defined as

$$\begin{aligned} \bar{\mathcal{G}} &\triangleq (A\bar{L}_1 + B\Sigma_1 \bar{\Lambda}_1)^\top \bar{P} (A\bar{L}_1 + B\Sigma_1 \bar{\Lambda}_1) + \bar{\mathcal{G}}_1^\top (\bar{T}_2 - \bar{T}_1) \bar{\mathcal{G}}_1 \\ &\quad + \bar{\mathcal{G}}_2^\top M_\Theta \bar{\mathcal{G}}_2 + \bar{\mathcal{G}}_3^\top \mathcal{M}_{\text{DNN}} \bar{\mathcal{G}}_3 + \text{Sym}(\bar{R}_1^\top \bar{R} \bar{R}_2 - \bar{R}_5^\top \bar{R} \bar{R}_6 \\ &\quad + \bar{N}_1 \bar{R}_9 + \bar{N}_2 \bar{R}_{10}) - \bar{R}_{11}^\top \bar{\Xi} \bar{R}_{11} - \bar{L}_1^\top \bar{P} \bar{L}_1, \\ \bar{\Pi}_1 &\triangleq \bar{\mathcal{G}}_1^\top \bar{T}_2 \bar{\mathcal{G}}_1 + \text{Sym}(\bar{R}_3^\top \bar{R} \bar{R}_7), \bar{\Pi}_2 \triangleq \bar{\mathcal{G}}_1^\top \bar{T}_1 \bar{\mathcal{G}}_1 + \text{Sym}(\bar{R}_8^\top \bar{R} \bar{R}_4). \end{aligned}$$

Note that the conditions $0 \leq k - k_q \leq s_k \leq \bar{s}$ and $0 < k_{q+1} - k \leq s_k \leq \bar{s}$ hold obviously within the time interval $[k_q, k_{q+1}-1]$, thus based on (Wan, Luan, Karimi, & Liu, 2021, Lemma 2), there exist scalars $\bar{\lambda}_i, i \in \mathbb{N}_{[1, 2]}$, such that the inequalities

$$\begin{aligned} (k - k_q) \text{Sym}(\bar{R}_3^\top \bar{R} \bar{R}_7) &\leq \bar{s} (\bar{\lambda}_1^{-1} \bar{R}_3^\top \bar{R} \bar{R}_3 + \bar{\lambda}_1 \bar{R}_7^\top \bar{R}_7), \quad (52) \\ (k_{q+1} - k) \text{Sym}(\bar{R}_8^\top \bar{R} \bar{R}_4) &\leq \bar{s} (\bar{\lambda}_2^{-1} \bar{R}_8^\top \bar{R} \bar{R}_8 + \bar{\lambda}_2 \bar{R}_4^\top \bar{R}_4), \quad (53) \end{aligned}$$

hold obviously. In addition, allowing for the terms $\bar{\mathcal{G}}_1^\top \bar{T}_i \bar{\mathcal{G}}_1 \succ 0$ for $i \in \mathbb{N}_{[1, 2]}$ with $\bar{T}_i \succ 0$, the conditions (51)-(53) yield

$$\begin{aligned} \left(\bar{\mathcal{G}} + \bar{s} (\bar{\mathcal{G}}_1^\top \bar{T}_2 \bar{\mathcal{G}}_1 + \bar{\mathcal{G}}_1^\top \bar{T}_1 \bar{\mathcal{G}}_1 + \bar{\lambda}_1 \bar{R}_7^\top \bar{R}_7 + \bar{\lambda}_2 \bar{R}_4^\top \bar{R}_4) \right. \\ \left. + \bar{s} (\bar{N}_1^\top \bar{T}_1^{-1} \bar{N}_1 + \bar{N}_2^\top \bar{T}_2^{-1} \bar{N}_2) + \bar{s} \bar{\lambda}_1^{-1} \bar{R}_3^\top \bar{R} \bar{R}_3 \right. \\ \left. + \bar{s} \bar{\lambda}_2^{-1} \bar{R}_8^\top \bar{R} \bar{R}_8 \right) \bar{\zeta}(k) < 0. \end{aligned} \quad (54)$$

Accordingly, by using Schur complement for (54), the first LMI in (40) can be obtained, which is convex for all decision variables. Besides, the feasibility of (54) implies that the condition (50) holds obviously. Note that the third term on the left side of (50) is greater than zero, allowing for the local sector quadratic constraint (16). Then, $\mathcal{S}(x(k_q), s_k) < 0$ holds during the execution interval $[k_q, k_{q+1}-1]$. We sum the remainder of (50) from $k = k_q$ to k_{q+1} , leading to

$$\begin{aligned} \sum_{k=k_q}^{k_{q+1}-1} (\Delta \bar{V}(\eta(k), k) + \|r(k) - r^*\|_{M_\Theta}^2) \\ = \bar{V}(\eta(k_{q+1})) - \bar{V}(\eta(k_q)) + \sum_{k=k_q}^{k_{q+1}} \|r(k) - r^*\|_{M_\Theta}^2 \end{aligned}$$

$$\leq -\bar{h}_2 \|\bar{\zeta}(k_q)\|^2 < 0, \quad (55)$$

which is satisfied for the looped function $\bar{W}(x(k_{q+1}), k_{q+1}) = \bar{W}(x(k_q), k_q)$ and $\bar{h}_2 \in \mathbb{R}_{>0}$. We generalize the time interval from $[k_q, k_{q+1}-1]$ to $[0, k_N]$ with $N \in \mathbb{N}_{>1}$. Letting $k_0=0$ and allowing for (55), we further obtain

$$\begin{aligned} & \sum_{q=0}^{N-1} (\bar{V}(\eta(k_{q+1})) - \bar{V}(\eta(k_q))) + \sum_{q=0}^{N-1} \sum_{k=k_q}^{k_{q+1}} \|r(k) - r^*\|_{M_\Theta}^2 \\ &= \bar{V}(\eta(k_N)) - \bar{V}(\eta(0)) + \sum_{k=0}^{k_N} \|r(k) - r^*\|_{M_\Theta}^2 \\ &\leq -\sum_{k=0}^{k_N} \bar{h}_2 \|\bar{\zeta}(k)\|^2. \end{aligned}$$

Note that $\sum_{k=0}^{k_N} \|r(k) - r^*\|_{M_\Theta}^2 \geq 0$ holds based on the definition of IQC in (4), which yields

$$\bar{V}(\eta(k_N)) - \bar{V}(\eta(0)) \leq -\sum_{k=0}^{k_N} \bar{h}_2 \|\bar{\zeta}(k)\|^2. \quad (56)$$

Hence, the asymptotical stability of $\bar{V}(\eta(k))$ is ensured, namely, $\eta(k)$ converges to η^* as k tends to ∞ . Similar to the proof as aforementioned, the second inequality of (40) shows the prerequisite of local quadratic constraint of π_{DNN} (16), that is, $p_1 \in [\underline{p}_1, \bar{p}_1]$ holds if $x(k) \in \mathcal{E}_{P_1}(x^*)$, in view of the constrained quadratic (Hindi & Boyd, 1998, Lemma 1) and the IBP specified in Remark 3. Thus, the local property is reasonable for self-triggered π_{DNN} .

We perform an inner-approximation of RoA based on the previous analysis. Recalling the inequality (56), it is intuitive that $\eta(k) \in \mathcal{E}_{\bar{P}}(\eta^*) \triangleq \{\eta \in \mathbb{R}^n \mid \|\eta - \eta^*\|_{\bar{P}}^2 \leq 1\}$ holds for an initial state $\eta(0) \in \mathcal{E}_{\bar{P}}(\eta^*)$. Based on the initial value $\xi(0)=0$ of virtual filter (3), we have that $\eta(0) \in \mathcal{E}_{\bar{P}}(\eta^*)$ yields $x(0) \in \mathcal{E}_{\bar{P}_1}(x^*)$, which is an inner approximation of robust RoA defined by (6), with \bar{P}_1 denoting the upper left block of \bar{P} . The proof is completed.

Similar to (35), the *largest* RoA estimation can be obtained by solving the optimization problem

$$\begin{aligned} & \min_{\bar{P} > 0, \bar{T}_z > 0, \bar{\Xi}_z > 0, \bar{\gamma} \geq 0, \bar{\lambda}_z \geq 0, \bar{R}, \bar{N}_z} \log(\text{Det}(\bar{P}_1)), \\ & \text{s.t. (40) holds,} \end{aligned} \quad (57)$$

which is convex about all decision variables defined in Theorem 2.

Remark 8 The upper bound \bar{p}_1 of the first-layer preactivation of π_{DNN} (7) explicitly affects the size of inner approximation of robust RoA as discussed in Remark 5. Different from the event-triggered scheme in Section 3, Theorem 2 captures the relation between the upper bound of transmission interval s_k and the feasibility of (57). Larger \bar{s} is conducive to reduce transmission times for improving communication efficiency, but the obtained RoA estimation may be more conservative at the cost of sacrificing a stability metric $\text{Det}(\bar{P}_1)$. In addition, the feasibility of (57) reveals that multiple self-triggered policies satisfying $s_k \leq \bar{s}$ will lead to

the same inner approximation of robust RoA $\mathcal{E}_{\bar{P}_1}(x^*)$, which implies more generality and flexibility. Considering a trade-off between communication burden and stability assessment, it is potential to capture the largest RoA approximation in view of determining the best upper bound \bar{s} of transmission intervals of self-triggered DNN control scheme (9).

Remark 9 We make discussions about the novelty of Theorem 2 in what follows, since fewer results have focused on designing self-triggered DNN control schemes. First, similar to Remark 6, the convex optimization (57) builds upon the association of the self-triggered transmissions (39) and the neural-feedback loops (5), leading to both better adaptivity to uncertainty impacts and more efficient communication transmission. Besides, we establish a relationship between the upper bound of self-triggered transmission intervals and the stability metric evaluated by $\text{Det}(P_1)$, which was not reported in the existing literature. Second, we consider the local sector-bounded attribute of nonlinear π_{DNN} and relax the nonlinearity to conduct the controller-dynamics association. Apart from the discussions in Remark 6, Theorem 2 well generalizes the linear case (Wang, Berberich, Sun, Wang, Allgöwer, & Chen, 2023, Section IV) to the nonlinear case, which also implies the potential of control synthesis of self-triggered system by virtue of nonlinearity cancellation/relaxation techniques (De Persis, Rotulo, & Tesi, 2023). Third, the LMI-based condition, verifying the closed-loop stability of self-triggered neural-feedback loops, is put forward to determine the triggering parameters in (37), where looped functions are utilized to reduce conservatism. Particularly, the strict stability criterion (40) for self-triggered logic (39) is proposed for the first time.

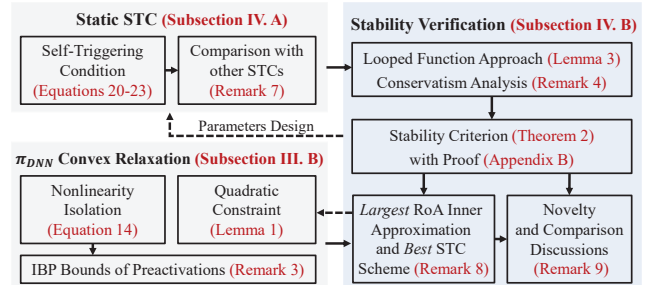


Fig. 3. The architecture of self-triggered neural control in Section 4.

Remark 10 We discuss the extensions of the technical results made above. First, considering the system without IQC filter (3), that is, $x(k+1) = A_\Gamma x(k) + B_\Gamma u(k) + F_\Gamma \omega(k)$ holds only with ω representing the bounded uncertainty/fault (Ma, Shi, & Wu, 2021), we still can perform stability analyses for aperiodic-sampled neural-feedback loops as Theorems 1 and 2, by virtue of replacing the matrices A and B with A_Γ and $[B_\Gamma \ F_\Gamma]$, while adjusting the dimensions of $L_\iota, \iota \in \mathbb{N}_{[1,8]}$ and $\bar{L}_{\bar{h}}, \bar{h} \in \mathbb{N}_{[1,7]}$, respectively. Note that the asymptotic stability degrades to the ultimate boundness, due to the existence of ω as (Ma, Shi, & Wu, 2021, Appendix A) and (Ye, Song, Zhang, & Wen, 2023, Theorem 1), which leads to a ro-

bust invariant set as $\overline{\mathcal{R}}_F \triangleq \{x_0 \in \mathbb{R}^n \mid \|\chi(\infty, x_0) - x^*\| \leq J(\bar{\omega})\}$ with $J(\bar{\omega})$ denoting a scalar function of the norm bound $\bar{\omega}$. It is possible to explore inner approximations of RoA based on the positive invariance of reachable sets. Second, apart from the LMI-based conditions herein, one can utilize convex relaxation of π_{DNN} combined with sums of squares optimization to determine inner approximations of RoA for a more general nonlinear systems, for example, the polynomial systems (Iannelli, Seiler, & Marcos, 2019, Algorithm 1). Moreover, the auxiliary looped-function approach herein can be leveraged in analyzing aperiodic-sampled neural-feedback loops based on the sums of squares optimization, which is consistent with (Iannelli, Seiler, & Marcos, 2019, Remark 2) and illuminates the future directions. Third, we suppose that the controller is pretrained by either imitating the experimental data pairs or approximating the model predictive control policy (Karg & Lucia, 2020), which is akin to use deterministic feedback control strategies to design aperiodic-sampled schemes (Wildhagen, Berberich, Hertneck, & Allgöwer, 2023). In practice, there exist suboptimal demonstrations and DNN approximation errors for training π_{DNN} (Drummond, Duncan, Turner, Pauli, & Allgöwer, 2022, Theorem 10), which influence setpoint tracking stability. Note that the loop transformation technique combined with the alternating direction method of multipliers algorithm, for example, (Yin, Seiler, Jin, & Arcak, 2022b, Section V) and (Pauli, Koch, Berberich, Kohler, & Allgöwer, 2021b, Section III), reveal a roadmap of learning π_{DNN} with closed-loop performance guarantees, which can be generalized to aperiodic-sampled communication transmissions, yielding a codesign of triggering logic and learning strategy. The relevant issues remain to be investigated in future works.

5 Numerical Simulation

In this section, the Euler discretization of inverted pendulum (De Persis, Rotulo, & Tesi, 2023, Example 1) is utilized to validate the effectiveness of our theoretical derivations. The numerical simulation is performed using `Matlab` with `CVX` toolkit and `MOSEK` solver. The codes are available at <https://github.com/Renjie-Ma/Aperiodic-Sampled-DNN-Controller.git>.

The inverted pendulum can be formulated by the interconnection of a nominal plant and an uncertainty part

$$\begin{aligned} x_1(k+1) &= x_1(k) + T_s x_2(k), \\ x_2(k+1) &= \frac{T_s g}{l_d} x_1(k) + \left(1 - \frac{T_s \mu}{m l_d^2}\right) x_2(k) + \frac{T_s}{m l_d^2} u(k) \\ &\quad - \frac{T_s g}{l_d} \omega(k), \\ \omega(k) &= x_1(k) - \sin(x_1(k)) = \Theta(\nu(k)), \end{aligned}$$

where T_s is the sampling time interval, g is the acceleration of gravity, l_d is the distance from the base to the center of mass of the balanced body, μ is the coefficient of

rotational friction, and m is the mass. The system state is $x = \text{Col}(x_1, x_2)$, where x_1 and x_2 denote the angular position and the velocity, respectively. We set $T_s = 0.01\text{s}$, $g = 9.80\text{m/s}^2$, $l_d = 0.50\text{m}$, $\mu = 0.05\text{Nms/rad}$, and $m = 0.15\text{kg}$ for the numerical simulation. We assume that $x_1(k) \in [\varphi, \bar{\varphi}]$ with $\bar{\varphi} = -\varphi = 0.73\text{rad}$ and $u(k) \in [\underline{u}, \bar{u}]$ with $\bar{u} = -\underline{u} = 0.7\text{Nm}$ hold in practice. The uncertainty Θ is locally sector-bounded by $\text{Sec}(\mathbf{I}_s, \mathbf{m}_s)$. Based on the definition of off-by-one IQC (Lessard et al., 2016, Lemma 8), we determine the parameters of virtual filter (3) by $A_\Phi = 0$, $B_\Phi = -\mathbf{I}_s$, $C_\Phi = \text{Col}(1, 0)$, $F_\Phi = 1$, $D_\Phi = \text{Col}(\mathbf{I}_s, -\mathbf{m}_s)$, and $G_\Phi = \text{Col}(-1, 1)$. Note that the physical constraints as aforementioned directly yield $\mathbf{l}_s = (\bar{\varphi} - \sin(\bar{\varphi})) / \bar{\varphi}$ and $\mathbf{m}_s = 0$. Thus, we can determine the system matrices of (5) accordingly.

The expert demonstrations can be obtained by solving an explicit model predictive control policy with `MPT3` toolkit. We fit the state-input data pairs by a DNN controller π_{DNN} (7), which is parameterized by two hidden layers $a_1 = 32$ and $a_2 = 32$ with `tanh` activation function. The training process is implemented via `PyTorch` in the same way as in (de Souza, Girard, & Tarbouriech, 2023). We assume that π_{DNN} is bias-free, and the neural-feedback loop (5) has a zero equilibrium as explained in Remark 3.

1) **Event-triggered scenario.** Based on the pretrained π_{DNN} , we compile the control policy in Subsection 3.3. The upper bound of sampling interval ϑ_u is set to be 5 for ensuring the feasibility of semidefinite programming (35). We specify the initial state by $\eta(0) = \text{Col}(0.19, 3.5, 0)$ and prescribe the scalars $\epsilon_1 = 0.003$ and $\epsilon_2 = 0.002$. Besides, the triggering parameters μ in (12) and g in (10) are set to be 0.05 and 500, respectively, such that the constraint $1 - \mu - g^{-1} \geq 0$ holds as analyzed in Remark 1. The state trajectories $\eta(k)$ of event-triggered neural-feedback loops (5) under different ϑ satisfying $1 = \vartheta_l \leq \vartheta \leq \vartheta_u$ can be illustrated in Fig. 4, in view of feasible solutions of triggering gains Ξ_1 and Ξ_2 in (11), where *Case 1*, *Case 2*, *Case 3*, and *Case 4* correspond to $\vartheta = 4, 3, 2, 1$, respectively. The simulation results reveal that the sampling intervals and their related triggering intervals degrade the closed-loop tracking stability as ϑ becomes larger. There is a tradeoff between communication efficiency and stability assurance, which is consistent with the theoretical analysis made in Remark 5. We cut out the event-triggered times and intervals for different ϑ in Fig. 5. For a complete time domain, the number of sampling times is 800, and the numbers of transmission instants are 179, 242, 351, and 739, which imply that communication efficiencies are improved by 77.63%, 69.75%, 56.13%, and 7.63%, respectively.

We assess the sizes of ellipsoidal inner-approximations of robust RoA for event-triggered neural-feedback loops in (5). First, we discuss the impacts induced by the local sector bound attribute $\text{Sec}[\rho, \sigma]$ of nonlinear DNN activation functions, which directly affects the feasible shape matrix P via semidefinite programming (35). In Fig. 6, we illustrate ellipsoidal inner approximations of robust RoA, introduced by Definition 2, with different bounds $(\delta_\rho, \delta_\beta)$ of the

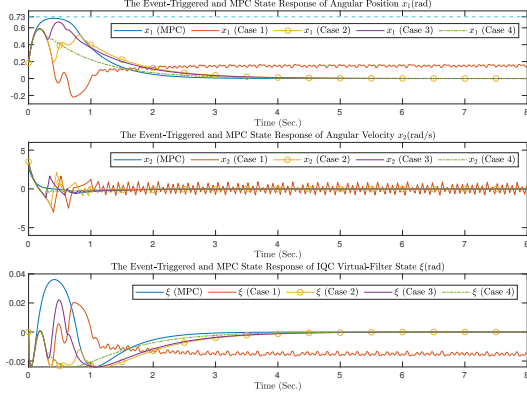


Fig. 4. The state trajectories of event-triggered neural-feedback loops (5) and MPC-feedback loops with the angular position x_1 , the angular velocity x_2 , and the IQC virtual filter state ξ .

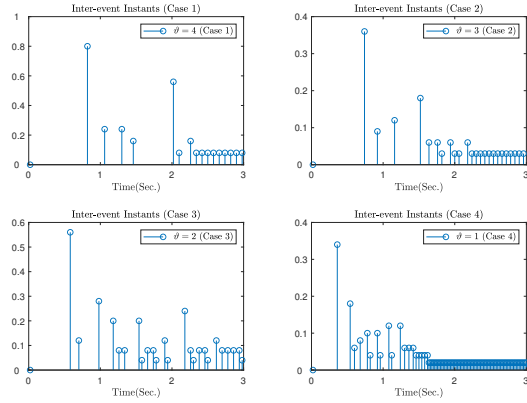


Fig. 5. The triggering instants and intervals of (13) corresponding to different constant sampling intervals ϑ .

first-layer DNN preactivation. We specify $p_1 \in [\underline{p}_1, \bar{p}_1]$ with $\bar{p}_1 = \underline{p}_1 = \delta_\rho \mathbf{1}_{a_1}$, in which $\delta_\rho \in \mathbb{R}_{(0,1)}$ and $\mathbf{1} \in \mathbb{R}^{a_1}$ whose elements are all ones. Based on IBP technique stated in Remark 3, we can calculate the term ρ and its related M_ρ in (16). For comparisons, δ_ρ can be selected by 0.25, 0.35, and 0.45 during the simulation. We prescribe the local upper bound $\sigma = \delta_\beta \mathbf{1}_{a_1}$, where δ_β can be selected by 0.97, 1.00, and 1.03, respectively. Fig. 6 mirrors the results corresponding to several combinations of δ_ρ and δ_β . The volumes of ellipsoidal RoA estimations are different, according to simulation results, the best choices leading to the *largest* RoA estimation are $\delta_\rho = 0.45$ and $\delta_\beta = 0.97$. Besides, compared to the simulation results in (de Souza, Girard, & Tarbouriech, 2023, Fig. 2), where the event-triggered scheme located within the interior of a DNN controller, we potentially enlarge the volumes while satisfying the physical constraint on the angular position x_1 . Hence, Fig. 6 is consistent with the theoretical discussions in Remark 5.

Besides, we also explore the impacts of sampling intervals on the inner approximations of robust RoA. Within this context, we prescribe the parameters of local sector bound of DNN

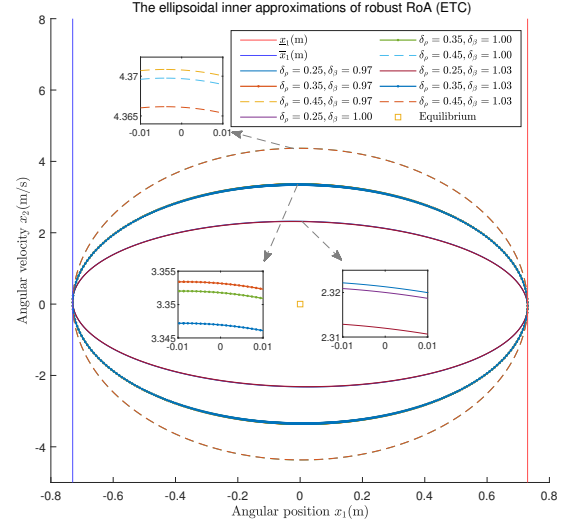


Fig. 6. The ellipsoidal inner approximations of robust RoA with different bounds $(\delta_\rho, \delta_\beta)$ of first-layer DNN preactivation under a fixed event-triggered transmission scheme.

by $(\delta_\rho, \delta_\beta) = (0.35, 1.00)$ for comparisons. According to the simulation results illustrated in Fig. 7, in which the RoA estimations with different ϑ satisfying $1 = \vartheta_l \leq \vartheta \leq \vartheta_u$ are plotted, we obtain that the size of ellipsoidal approximation is decrescent when the sampling interval ϑ becomes larger. Albeit increasing the value of ϑ is beneficial for reducing the computation burden, the size of RoA inner approximation, acting as a stability metric, can be contractible, which also reveals a tradeoff as in Remark 5.

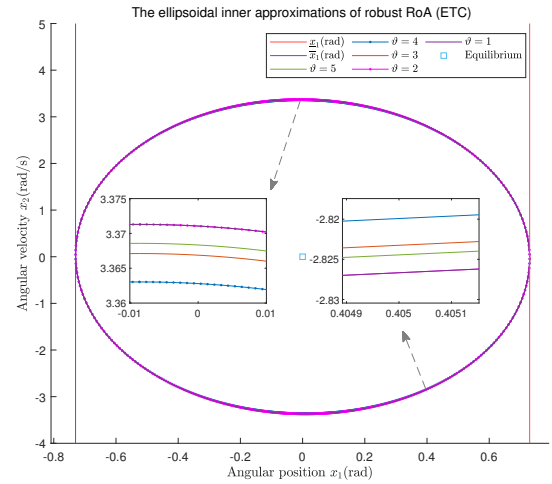


Fig. 7. The ellipsoidal inner approximations of robust RoA under different sampling intervals ϑ of event-triggered transmissions.

2) Self-triggered scenario. Based on a pretrained π_{DNN} , we execute the control policy in Subsection 4.2. The self-triggered parameters are prescribed with $\bar{\epsilon}_1 = 0.8$, $\bar{\epsilon}_2 = 0.6$, and $\bar{s} = 10$. By solving the semidefinite programming

problem (57), we obtain the feasible solutions $\tilde{\Xi}_1$ and $\tilde{\Xi}_2$ in (38). The closed-loop state trajectories $\eta(k)$ of self-triggered neural-feedback loops (5) under different initial conditions are illustrated in Fig. 8, in which *Case 1*, *Case 2*, and *Case 3* correspond to the initial states $\text{Col}(0.19, 3.5, 0)$, $\text{Col}(0.43, 3.0, 0)$, and $\text{Col}(-0.33, -3.3, 0)$, respectively. The effectiveness of self-triggered DNN controller to stabilize the system (5) is verified. We illustrate self-triggered times and intervals of (39) in Fig. 9. The number of time steps is 800, and the numbers of triggered times are 222, 219, and 218, such that the communication efficiencies are 72.25%, 72.63%, and 72.75%, respectively. Thus, the self-triggered DNN controller is resource-efficient while ensuring the setpoint tracking stability.

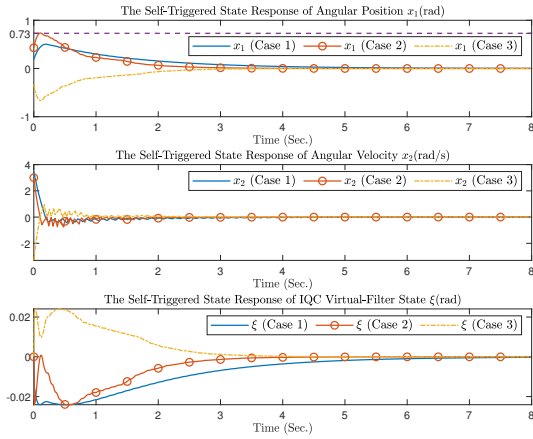


Fig. 8. The state trajectories of self-triggered neural-feedback loops (5) with the angular position x_1 , the angular velocity x_2 , and the IQC virtual filter state ξ .

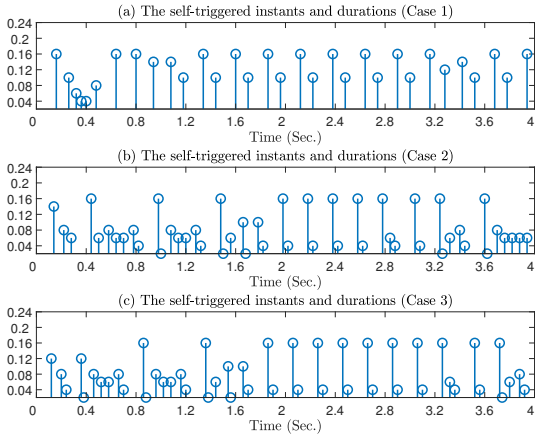


Fig. 9. The self-triggered times and intervals of (39) corresponding to different initial states

We then assess the sizes of ellipsoidal inner-approximations of robust RoA for the self-triggered neural-feedback loops (5). As we discussed in Remark 8, the feasibility of ellipsoidal shape matrix \bar{P} in (57) leads to a same inner approximation of robust RoA $\mathcal{E}_{\bar{P}_1}(x^*)$ for $s_k \leq \bar{s}$. We only need

to compare RoA estimations corresponding to different local sector bounds of DNNs. We illustrate the simulation results in Fig. 10, based on which, the *largest* RoA estimation matches the selection $\delta_\rho = 0.45$ and $\delta_\beta = 1.03$. Moreover, we also notice that the volumes of ellipsoidal RoA estimations are increased, as δ_ρ becomes larger to some extent, and are related with the preactivation bounds of DNNs. The simulation results are consistent with the discussions in Subsection 4.2.

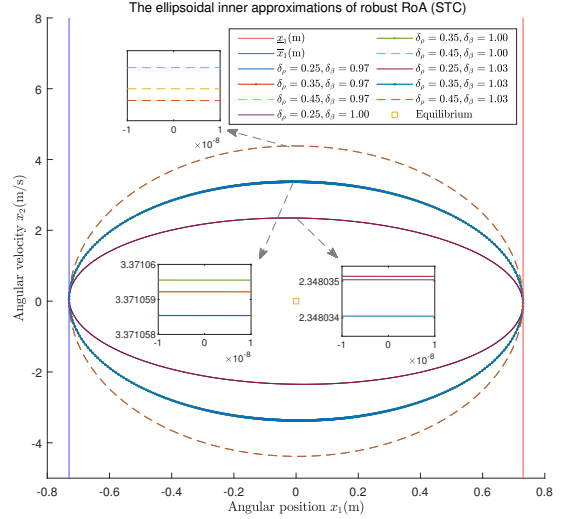


Fig. 10. The ellipsoidal inner approximations of robust RoA with different bounds $(\delta_\rho, \delta_\beta)$ of first-layer DNN preactivation under a fixed self-triggered transmission scheme.

6 Conclusion

This paper has investigated aperiodic-sampled DNN control schemes for a class of uncertain systems, whose setpoint tracking stability can be strictly ensured. Firstly, both event- and self-triggered schemes were incorporated with neural-feedback loops to determine the communication transmission instants. Then, the quadratic constraint of DNN, based on the local sector-bounded specifications of activation functions, and the auxiliary looped functions were utilized for deriving the stability guarantees, leading to convex programming problems, whose feasible solutions can be utilized to design the triggering parameters. Besides, we assessed the sizes of ellipsoidal RoA inner approximations, acting as a stability metric, which can be correlated with the triggering logics and the local attributes of DNN activation functions. Finally, we provided a numerical example of an inverted pendulum to validate the effectiveness of theoretical derivations herein.

Acknowledgements

The authors sincerely thank Prof. Dr. Marios M. Polycarpou from the University of Cyprus and Prof. Dr. Luca Zaccarian from the LAAS-CNRS, University of Toulouse, CNRS

for their valuable suggestions and fruitful discussions in the research. We also thank Mr. Su Zhang and Mr. Zeyu Wang for their contributions in numerical simulations.

References

- Akashi, S., Ishii, H., & Cetinkaya, A. (2018). Self-triggered control with tradeoffs in communication and computation. *Automatica*, 94, 373–380.
- Cao, Z., Niu, Y., & Zou, Y. (2023). Self-triggered multi-mode control of markovian jump systems. *Automatica*, 149, 110837.
- Chen, J., Xu, S., Jia, X., & Zhang, B. (2016). Novel summation inequalities and their applications to stability analysis for systems with time-varying delay. *IEEE Transactions on Automatic Control*, 62 (5), 2470–2475.
- Coutinho, P. H. S., & Palhares, R. M. (2022). Codesign of dynamic event-triggered gain-scheduling control for a class of nonlinear systems. *IEEE Transactions on Automatic Control*, 67 (8), 4186–4193.
- D’Amico, W., La Bella, A., & Farina, M. (2024). An incremental input-to-state stability condition for a class of recurrent neural networks. *IEEE Transactions on Automatic Control*, 69 (4), 2221–2236.
- De Persis, C., Rotulo, M., & Tesi, P. (2023). Learning controllers from data via approximate nonlinearity cancellation. *IEEE Transactions on Automatic Control*, 68 (10), 6082–6097.
- de Souza, C., Girard, A., & Tarbouriech, S. (2023). Event-triggered neural network control using quadratic constraints for perturbed systems. *Automatica*, 157, 111237.
- Drummond, R., Duncan, S., Turner, M., Pauli, P., & Allgöwer, F. (2022). Bounding the difference between model predictive control and neural networks. In: 4th Learning for Dynamics and Control Conference. PMLR, pp. 817–829.
- Fabiani, F., & Goulart, P. J. (2023). Reliably-stabilizing piecewise-affine neural network controllers. *IEEE Transactions on Automatic Control*, 68 (9), 5201–5215.
- Fazlyab, M., Morari, M., & Pappas, G. J. (2022). Safety verification and robustness analysis of neural networks via quadratic constraints and semidefinite programming. *IEEE Transactions on Automatic Control*, 67 (1), 1–15.
- Fazlyab, M., Robey, A., Hassani, H., Morari, M., & Pappas, G. (2019). Efficient and accurate estimation of lipschitz constants for deep neural networks. *Advances in Neural Information Processing Systems*, 32, 11427–11438.
- Gates, O., Newton, M., & Gatsis, K. (2023). Scalable forward reachability analysis of multi-agent systems with neural network controllers. In: 62nd IEEE Conference on Decision and Control. IEEE, pp. 67–72.
- Ghodrat, M., & Marquez, H. J. (2023). A new lyapunov-based event-triggered control of linear systems. *IEEE Transactions on Automatic Control*, 68 (4), 2599–2606.
- Girard, A. (2015). Dynamic triggering mechanisms for event-triggered control. *IEEE Transactions on Automatic Control*, 60 (7), 1992–1997.
- Gowal, S., Dvijotham, K., Stanforth, R., Bunel, R., Qin, C., Uesato, J., Arandjelovic, R., Mann, T., & Kohli, P. (2018). On the effectiveness of interval bound propagation for training verifiably robust models. *arXiv preprint arXiv:1810.12715*.
- Heemels, W. P., Johansson, K. H., & Tabuada, P. (2012). An introduction to event-triggered and self-triggered control. In: 51st IEEE Conference on Decision and Control. IEEE, pp. 3270–3285.
- Hindi, H., & Boyd, S. (1998). Analysis of linear systems with saturation using convex optimization. In: 37th IEEE Conference on Decision and Control. IEEE, pp. 903–908.
- Hu, B., Lacerda, M. J., & Seiler, P. (2017). Robustness analysis of uncertain discrete-time systems with dissipation inequalities and integral quadratic constraints. *International Journal of Robust and Nonlinear Control*, 27 (11), 1940–1962.
- Hu, H., Fazlyab, M., Morari, M., & Pappas, G. J. (2020). Reach-sdp: Reachability analysis of closed-loop systems with neural network controllers via semidefinite programming. In: 59th IEEE conference on decision and control. IEEE, pp. 5929–5934.
- Hu, Z., Su, R., Veerasamy, V., Huang, L., & Ma, R. (2025). Resilient frequency regulation for microgrids under phasor measurement unit faults and communication intermittency. *IEEE Transactions on Industrial Informatics*, 21 (2), 1941–1949.
- Iannelli, A., Seiler, P., & Marcos, A. (2019). Region of attraction analysis with integral quadratic constraints. *Automatica*, 109, 108543.
- Jin, M., & Lavaei, J. (2018). Control-theoretic analysis of smoothness for stability-certified reinforcement learning. In: 57th IEEE Conference on Decision and Control. IEEE, pp. 6840–6847.
- Karg, B., & Lucia, S. (2020). Efficient representation and approximation of model predictive control laws via deep learning. *IEEE Transactions on Cybernetics*, 50 (9), 3866–3878.
- La Bella, A., Farina, M., D’Amico, W., & Zaccarian, L. (2025). Regional stability conditions for recurrent neural network-based control systems. *Automatica*, 174, 112127.
- Lessard, L., Recht, B., & Packard, A. (2016). Analysis and design of optimization algorithms via integral quadratic constraints. *SIAM Journal on Optimization*, 26 (1), 57–95.
- Li, X., Wang, Y., & Song, S. (2023). Stability of nonlinear impulsive systems: Self-triggered comparison system approach. *IEEE Transactions on Automatic Control*, 68 (8), 4940–4947.
- Liu, Q., Wang, Z., He, X., & Zhou, D.-H. (2015). Event-based recursive distributed filtering over wireless sensor networks. *IEEE Transactions on Automatic Control*, 60 (9), 2470–2475.
- Ma, R., & Hu, Z. (2024). Deep neural network-controlled safety-critical systems with uncertainty resilience. *IEEE Internet of Things Journal*, 11 (13), 24061–24072.
- Ma, R., Shi, P., & Wu, L. (2021). Sparse false injection attacks reconstruction via descriptor sliding mode observers. *IEEE Transactions on Automatic Control*, 66 (11), 5369–5376.
- Nino, C. F., Patil, O. S., Insinger, J. C., Eisman, M. R., &

- Dixon, W. E. (2025). Online resnet-based adaptive control for nonlinear target tracking. *IEEE Control Systems Letters*, DOI: 10.1109/LCSYS.2025.3576652.
- Pauli, P., Köhler, J., Berberich, J., Koch, A., & Allgöwer, F. (2021)a. Offset-free setpoint tracking using neural network controllers. In: 3rd Learning for dynamics and control Conference. PMLR, pp. 992–1003.
- Pauli, P., Koch, A., Berberich, J., Kohler, P., & Allgöwer, F. (2021)b. Training robust neural networks using lipschitz bounds. *IEEE Control Systems Letters*, 6, 121–126.
- Peng, C., & Han, Q.-L. (2016). On designing a novel self-triggered sampling scheme for networked control systems with data losses and communication delays. *IEEE Transactions on Industrial Electronics*, 63 (2), 1239–1248.
- Ragunathan, A., Steinhardt, J., & Liang, P. S. (2018). Semidefinite relaxations for certifying robustness to adversarial examples. *Advances in neural information processing systems*, 31, 10900–10910.
- Schwenkel, L., Köhler, J., Müller, M. A., & Allgöwer, F. (2023). Model predictive control for linear uncertain systems using integral quadratic constraints. *IEEE Transactions on Automatic Control*, 68 (1), 355–368.
- Seifullae, R., Knorn, S., & Ahlén, A. (2022). Event-triggered control of systems with sector-bounded nonlinearities and intermittent packet transmissions. *Automatica*, 146, 110651.
- Seiler, P. (2015). Stability analysis with dissipation inequalities and integral quadratic constraints. *IEEE Transactions on Automatic Control*, 60 (6), 1704–1709.
- Seuret, A. (2012). A novel stability analysis of linear systems under asynchronous samplings. *Automatica*, 48 (1), 177–182.
- Talukder, S., & Kumar, R. (2023). Robust stability of neural-network-controlled nonlinear systems with parametric variability. *IEEE Transactions on Systems, Man, and Cybernetics: Systems*, 53 (8), 4820–4832.
- Tripathy, N. S., Kar, I., & Paul, K. (2017). Stabilization of uncertain discrete-time linear system with limited communication. *IEEE Transactions on Automatic Control*, 62 (9), 4727–4733.
- Valmorbida, G., & Anderson, J. (2017). Region of attraction estimation using invariant sets and rational lyapunov functions. *Automatica*, 75, 37–45.
- Wakaiki, M. (2023). Self-triggered stabilization of discrete-time linear systems with quantized state measurements. *IEEE Transactions on Automatic Control*, 68 (3), 1776–1783.
- Wan, H., Luan, X., Karimi, H. R., & Liu, F. (2021). Dynamic self-triggered controller codesign for markov jump systems. *IEEE Transactions on Automatic Control*, 66 (3), 1353–1360.
- Wang, X., Berberich, J., Sun, J., Wang, G., Allgöwer, F., & Chen, J. (2023). Model-based and data-driven control of event-and self-triggered discrete-time linear systems. *IEEE Transactions on Cybernetics*, 53 (9), 6066–6079.
- Wildhagen, S., Berberich, J., Hertneck, M., & Allgöwer, F. (2023). Data-driven analysis and controller design for discrete-time systems under aperiodic sampling. *IEEE Transactions on Automatic Control*, 68 (6), 3210–3225.
- Wong, E., & Kolter, Z. (2018). Provable defenses against adversarial examples via the convex outer adversarial polytope. In: 35th International Conference on Machine Learning. PMLR, pp. 5286–5295.
- Xiang, W., Tran, H.-D., Yang, X., & Johnson, T. T. (2021). Reachable set estimation for neural network control systems: A simulation-guided approach. *IEEE Transactions on Neural Networks and Learning Systems*, 32 (5), 1821–1830.
- Ye, H., Song, Y., Zhang, Z., & Wen, C. (2023). Global dynamic event-triggered control for nonlinear systems with sensor and actuator faults: A matrix-pencil-based approach. *IEEE Transactions on Automatic Control*, 69 (3), 2007–2014.
- Yin, H., Seiler, P., & Arcak, M. (2022)a. Stability analysis using quadratic constraints for systems with neural network controllers. *IEEE Transactions on Automatic Control*, 67 (4), 1980–1987.
- Yin, H., Seiler, P., Jin, M., & Arcak, M. (2022)b. Imitation learning with stability and safety guarantees. *IEEE Control Systems Letters*, 6, 409–414.
- Zhao, R., Zuo, Z., & Wang, Y. (2022). Event-triggered control for switched systems with denial-of-service attack. *IEEE Transactions on Automatic Control*, 67 (8), 4077–4090.